Global vegetation variability and its response to elevated CO_2, global warming, and climate variability - A study using the offline SSiB4/TRIFFID model and satellite data

Ye Liu[1], Yongkang Xue[1*], Glen MacDonald[1], Peter Cox[2], Zhengqiu Zhang[3]

[1] University of California Los Angeles (UCLA), Los Angeles, CA, USA
[2] College of Engineering, Mathematics and Physical Science, University of Exeter, Exeter, UK
[3] Chinese Academy of Meteorological Sciences, Beijing, China

Correspondence to: Yongkang Xue (yxue@geog.ucla.edu)

Submitted to Earth System Dynamics

October 15, 2018

Abstract. The climate regime shift during the 1980s had a substantial impact on the terrestrial ecosystems and vegetation at different scales. However, the mechanisms driving vegetation changes, before and after the shift, remain unclear. In this study, we used a biophysical-dynamic vegetation model to estimate large-scale trends in terms of carbon fixation, vegetation growth and expansion during the period 1958-2007, and to attribute these changes to environmental drivers including elevated atmospheric CO_2 concentration (hereafter eCO_2), global warming, and climate variability (hereafter CV). Simulated Leaf Area Index (LAI) and Gross Primary Product (GPP) were evaluated against observation-based data. Significant spatial correlations are found (correlations>0.87), along with regionally varying temporal correlations of 0.34-0.80 for LAI and 0.45-0.83 for GPP. More than 40% of the global land area shows significant positive (increase) or negative (decrease) trends in LAI and GPP during 1958-2007. Regions over globe show different characteristics in terms of ecosystem trends before and after the 1980s. While 11.7% and 19.3% of land has consistently positive LAI and GPP trends respectively, since 1958; 17.1% and 20.1% of land, saw LAI and GPP trends, respectively, reverse during the 1980s. Vegetation fraction cover (FRAC) trends, representing vegetation expansion/shrinking, are found at the edges of semi-arid areas and polar areas. Environmental drivers affect the change in ecosystem trend over different regions. Overall, eCO_2 consistently contributes to positive LAI and GPP trends in the tropics. Global warming mostly affects LAI, with positive effects in high latitudes and negative effects in subtropical semi-arid areas. CV is found to dominate the variability of FRAC, LAI, and GPP in the semi-humid and semi-arid areas. The eCO_2 and global warming effects increased after the 1980s, while the CV effect reversed during the 1980s. In addition, plant competition is shown to have played an important role in determining which driver dominated the regional trends. This paper presents a new insight into ecosystem variability and changes in the varying climate since the 1950s.

Keywords: Ecosystem variability, dynamic vegetation modelling, elevated CO_2, global warming, climate change and variability, TRIFFID, SSiB

1 Introduction

Climate variability and change, including global warming, and elevated atmospheric CO_2 concentrations (referred to as eCO_2 in this paper), have profound impacts on the terrestrial biosphere at global and regional scales (Garcia et al., 2014); while the terrestrial biosphere, in turn, affects the global climate by altering the exchanges of carbon, water and energy between the atmosphere and land surface (Cox et al., 2000; Xue et al., 2004, 2010; Friedlingstein et al., 2006; Ma et al., 2013). Important trends in terrestrial ecosystem carbon fixation, growth, and expansion in the past 60 years have been detected (Myneni et al., 1997; Piao et al., 2011, 2015; Ichii et al., 2013; Los 2013; Zhu et al., 2016). For instance, general earth greening has been discovered by analysing satellite-derived Normalized Difference Vegetation Index (NDVI) (Myneni et al., 1997; Piao et al., 2011; Ichii et al., 2013; Los 2013) and Leaf Area Index (LAI, defined as the one-side leaf area per ground area) products (Piao et al., 2011, 2015; Zhu et al., 2016). The Earth's terrestrial vegetation has acted as an important carbon sink in the past 60 years (Ballantyne et al., 2012; Le Quéré et al., 2013), with a significantly strengthening carbon sink rate, about 0.06 PgC/yr^{-2}, after the 1980s (Sitch et al., 2015), revealing growth in plant productivity (Nemani et al., 2003; Anav et al., 2015). In the meantime, vegetation fractional coverage (hereafter FRAC) has been changing, including some large-scale increases in total vegetation cover (Piao et al., 2005; Donohue et al., 2009; McDowell et al., 2015), and shifts in the spatial distributions of plants species, such as woody plants encroachment in the savanna area (Stevens et al., 2017) and shrubification in the tundra biome (Epstein et al., 2012; Mod and Luoto, 2016).

Many studies have attributed these large-scale ecosystem trends to climatic drivers and eCO_2 after applying statistical methods to satellite-based observations or the results from process-based land surface models (Myneni et al., 1997; Liu et al., 2006; Ichii et al., 2013; Mao et al., 2013; Piao et al., 2015; Schimel et al., 2015; Sitch et al., 2015; Devaraju et al., 2016; Zhu et al., 2016; Smith et al., 2016). Statistical regression and cross-correlation have been applied to attribute the recent biosphere changes to precipitation, temperature, and solar radiation variability (Zeng et al., 2013; Myers-Smith et al., 2015). Results from these studies indicated that northern mid- to high- latitude NDVI anomalies were positively correlated with temperature, and positively associated with precipitation in temperate to tropical semi-arid and arid regions (Zeng et al., 2013). However, statistical methods rarely isolate the drivers'

contribution to the inter-annual or decadal variability of the terrestrial ecosystem (Ahlbeck, 2002; Piao et al., 2015). Moreover, satellite products only cover the period after 1980 (Zhu et al., 2013).

Process-based land surface models overcome these limitations and are also able to include atmospheric CO_2 as an external driver. Dynamic Global Vegetation Models (DGVMs) simulated vegetation cover changes in response to changes in climate and atmospheric CO_2, and update associated surface characteristics such as PFT distribution and LAI (Claussen and Gayler, 1997; Smith et al., 2001; Bonan et al., 2002; Sitch et al., 2003; Woodward and Lomas, 2004; Krinner et al., 2005; Zeng et al., 2005; Zaehle and Friend, 2010; Lawrence et al., 2011; Zhang et al., 2015). By applying DGVMs in a model intercomparison project (called TRENDY), a general consensus has been reached that eCO_2 explains the greater part of the increasing trend of LAI and GPP towards the end of the 1980s (Schimel et al., 2015; Sitch et al., 2015; Zhu et al., 2016). Air temperature, precipitation, land use and land cover change, and nitrogen decomposition, also play roles in the changing terrestrial biosphere (Cramer et al., 2001; Schimel et al., 2015; Zhu et al., 2016). However, DGVMs should be applied with caution. The Coupled Model Intercomparison Project Phase 5 (CMIP5) reported that most DGVMs overestimated LAI in comparison to Global Inventory Monitoring and Modeling System (GIMMS) data (Murray-Tortarolo et al., 2013; Zhu et al., 2013). In addition, large discrepancies between models were found when predicting ecosystem variability and trends (Piao et al., 2013; Zhu et al., 2017). Unsurprisingly, the dominant factors obtained from different models are often significantly different (Beer et al., 2010; Huntzinger et al., 2017). Furthermore, DGVM simulations were sensitive to meteorological forcing data (Slevin et al., 2017; Wu et al., 2017). Therefore, a comprehensive evaluation of large-scale terrestrial ecosystem vegetation trends and potential drivers is crucial for improved DGVM application.

Most ecosystem trend detection and attribution studies have focused on the period after the 1980s when satellite data has been available (Myneni et al, 1997; Schimel et al., 2015; Zhu et al., 2015). However, a climate regime shift, identified by abrupt shifts in temperature, precipitation, and other climate variables (e.g. wind speed and sea surface pressure), was observed during the 1980s (Gong and Ho, 2002; Lo and Hsu, 2010; Reid et al., 2016). The responses of vegetation to these climate shifts have not yet been comprehensively investigated, especially at the level of individual Plant Function Types (PFTs).

In this study, we investigate the effect of eCO_2 and climate drivers including global warming and climate variability (i.e., meteorological forcing excluding global warming, referred to as "CV") on the trends of FRAC, LAI, and GPP during the period 1958-2007 by using the SSiB4/TRIFFID (Simplified Simple Biosphere model version 4/Top-down Representation of Interactive Foliage and Flora Including Dynamics) DGVM (Xue et al., 1991; Cox, 2001; Zhan et al., 2003; Zhang et al., 2015; Harper et al., 2016) at both grid and PFT levels, and using satellite products whenever they are available. Changes in the ecosystem trends are attributed to changes in eCO_2 and climate effects, focusing particularly on the climate regime shift during the 1980s. The key focuses of this paper are on 1) how the vegetation trends change before and after the 1980s; and 2) What is the effect of climate regime shifts during the 1980s on the vegetation trend before/after the 1980s.

2. Model description, experimental design and data

2.1 Model description

The Simplified Simple Biosphere model (SSiB) is a biophysically based model which simulates fluxes of radiation, momentum, sensible heat, and latent heat, as well as runoff, soil moisture, and surface temperature (Xue et al., 1991). A photosynthesis model (Collatz et al., 1991, 1992) has been implemented into SSiB to calculate carbon assimilation, forming SSiB2 (Zhan et al., 2003). The TRIFFID DGVM (Cox, 2001) was coupled to SSiB version 4 (Xue et al., 2006) to calculate vegetation dynamics, including relevant land-surface characteristics of vegetation cover and structure. Zhang et al. (2015) updated the competition dominance hierarchy from tree-shrub-grass (i.e., trees dominate shrubs and grasses, and shrubs dominate grasses) to tree-grass-shrub, but still allowed shrubs and grasses to compete for sunshine and space. SSiB4 estimates net plant photosynthesis assimilation rate, autotrophic respiration and other surface conditions such as canopy temperature and soil moisture for TRIFFID. TRIFFID updates the coverage of a PFT based on the net carbon available to it and the competition with other PFTs, which is controlled by the Lotka-Volterra equations. Vegetation is descripted by leaf, wood, and root with associating carbon pools. Leaf phenology is simulated as a function of canopy temperature and soil moisture. In addition, tundra was separated from the original single shrub category in order to better

reflect the arctic biomes. Evergreen and deciduous broadleaf trees are also separated as different PFTs. To date, SSiB4/TRIFFID therefore includes 7 PFTs: 1) Evergreen broadleaf trees, 2) Deciduous broadleaf trees, 3) Needle leaf broadleaf trees, 4) C3 grasses, 5) C4 plants, 6) Shrubs, and 7) Tundra.

2.2 Experimental design

In this study, SSiB4/TRIFFID was used to simulate the global vegetation distribution and assess the sensitivity of ecosystem trends to climate and eCO_2. Two sets of simulations were performed: 1) a 100-year quasi-equilibrium simulation driven by climatological forcing, and 2) sensitivity simulations driven by real-forcing from 1948-2007 (**Table 1**). In the first set, SSiB4/TRIFFID was driven with the climatological forcing and 1948 CO_2 concentration to reach a steady state, which was used as the initial condition in the second set of simulations.

Using the quasi-equilibrium simulation results as the initial condition, the historical meteorological forcing and yearly updated atmospheric CO_2 concentration were used to drive SSiB4/TRIFFID from 1948 through 2007. In this control simulation, we evaluated the model performance in reproducing the climatology and variability of vegetation coverage, LAI and GPP in comparison with multiple observation-based datasets. The long-term trends were diagnosed before and after the climate regime shift of the 1980s. Furthermore, three sets of experiments were conducted to quantify the effects of environmental drivers (climate and CO_2) and vegetation competition on the ecosystem trends. These experiments were designed as following:

1. Fixed-CO_2: The model was driven by the same meteorological forcing as the control experiment, but CO_2 concentration was fixed at the level of 1948 (310.33 ppm). The difference between control experiment and Fixed-CO_2 indicates the eCO_2 effect.
2. Detrend-Temp: The mean warming trend over each 10 degrees of latitude, from 1948 to 2007, was subtracted in this experiment. Then the detrended temperature along with other meteorological forcing and annually varying CO_2 concentration were used to drive the model. Subtraction of Detrend-Temp from the control experiment isolates the effect of global warming.
3. Climate Variability: Subtraction of both Fixed-CO_2 and Detrend-Temp from the control experiment was regarded as representing the effect of CV.

2.3 Data

A SSiB vegetation and soil map is used as the preliminary initial condition for the quasi-equilibrium simulation. A 3-hourly meteorological forcing data from 1948 through 2007 (Sheffield et al., 2006) is used for this study. The observation-based LAI and GPP products (Zhu et al., 2013; Xiao et al., 2014; Jung et al., 2009) are used to validate and calibrate the model to produce proper vegetation spatial distribution and temporal variability.

2.3.1 Initial condition for equilibrium simulation

There are different ways to initialize the surface condition for the quasi-equilibrium simulation. Based on our previous study (Zhang et al., 2015), we set up the initial condition using the SSiB vegetation map and SSiB vegetation table, which are based on ground survey and satellite-derived information (Dorman and Sellers, 1989; Xue et al., 2004b; Zhang et al., 2015) with 100% occupation at each grid point for the dominant PFT and zero for other PFTs.

2.3.2 Meteorological forcing data

The Princeton global meteorological dataset version 1 for land surface modelling (Sheffield et al., 2006) is used to drive SSiB4/TRIFFID for the period of 1948-2007. This dataset is constructed by combining a suite of global observation-based datasets with the National Centers for Environmental Prediction–National Center for Atmospheric Research (NCEP–NCAR) reanalysis starting from 1948 (http://hydrology.princeton.edu/data/pgf/). The spatial resolution is 1^o x 1^o and temporal interval is 3-hourly. This dataset, including surface air temperature (K), pressure (Pa), specific humidity (g/kg), wind speed (m/s), downward short-wave radiation flux (W/m^2), downward long-wave radiation flux (W/m^2), and precipitation (mm/day). Its 60-year mean climatology with three-hour interval from January 1 through December 31 was generated to drive quasi-equilibrium simulation.

2.3.3 Observation-based data

Two satellite-derived global land cover maps are used to evaluate the vegetation distribution in both quasi-equilibrium and real-forcing simulations. The Global Land Cover (GLC) database for the year 2000 (Bartholome et al., 2002) is used that was derived from Satellite Poul l'Observation de la Terre at the

spatial resolution about 1 km. This dataset provides a global map with one consistent legend, as well as regional maps with separate legends containing more detail for certain regions. For instance, tundra is not included in the global legend but is included in the regional product for Northern Eurasia (Bartalev et al., 2003). The regional land cover maps (download from http://forobs.jrc.ec.europa.eu/products/glc2000/glc2000.php) are used to calculate the land cover fraction by counting the percentage of each PFT in a 1-degree grid, then are merged to form a global land cover fraction map. Other than GLC2000, the Land Cover Type Climate Modeling Grid (CMG) product (MCD12C1), which is derived using the same algorithm that produces the V051 Global 500 m Land Cover Type product (MCD12Q1) from the observation input of Terra and Aqua on board the Moderate Resolution Imaging Spectroradiometer (MODIS), is also used as a reference (Friedl et al., 2010). The MODIS-MCD12C1 product provides land cover fraction at the spatial resolution of 0.05^{o}, which then converted to 1-degree resolution. The SSiB4/TRIFFID only includes primary land cover types, while both GLC2000 and MODIS IGBP have more sublevel classes. For easy comparison of the distribution of dominant vegetation types with different products, we hierarchically combine the GLC2000 and the MODIS IGBP classifications to the SSiB4/TRIFFID PFTs.

To assess the climatology, variation, and trends of simulated LAI, two widely used LAI products were used as references in this study: the Global Inventory Modelling and Mapping Studies (GIMMS) LAI (refer to LAI3g, the third generation, Zhu et al., 2013) was downloaded from https://ecocast.arc.nasa.gov/data/pub/gimms. A neural network algorithm was trained to using the AVHRR GIMMS NDVI3g (covering the period July 1981 to December 2011) and best-quality Terra MOIDS LAI (covering the period 2000 to 2009) for the overlapping period 2000-2009. Then the trained neural network algorithm was used to generate corresponding LAI dataset at 15-day temporal resolution and 1/12-degree spatial resolution for the period from July 1981 to December 2011. The Global Land Surface Satellite (GLASS) LAI was downloaded from http://www.bnu-datacenter.com. The GLASS LAI was generated from AVHRR reflectance (1982-1999) and MODIS reflectance (2000-2012) (Xiao et al., 2014). The GLASS LAI provides observations at 8-day temporal resolution and 1 km spatial resolution for the period from 1982 to 2012. Both datasets have general consistence in LAI spatial distribution, however, GIMMS shows 25% of the vegetated areas are greening during the 1982 to 2009, whereas 50%

in GLASS LAI (Zhu et al., 2016). GIMMS and GLASS LAI, and the meteorological forcing data for overlap period 1982 to 2007, were resampled to 1-degree spatial resolution and a monthly temporal interval.

SSiB4/TRIFFID GPP was evaluated using the FLUXNET-MTE GPP, which was downloaded from https://www.bgc-jena.mpg.de/geodb/projects/Data.php. The FLUXNET-MTE GPP was upscaled from FLUXNET observations of carbon dioxide flux to the global scale using the machine learning technique, model tree ensembles (MTE). This method was trained to predict site-level GPP based on remote sensing indices, climate and meteorological data, and information on land use (Jung et al., 2009). This data set provides global monthly mean GPP at 0.5-degree spatial resolution for the period from 1982 to 2011. The FLUXNET-MTE GPP was resampled to 1-degree spatial and monthly temporal resolution.

3. Results

3.1 Vegetation initial conditions

The DGVM's initial conditions for long-term simulations is obtained from a quasi-equilibrium solution in a long term simulation using the climatological forcing as presented in Section 2.3.2. The effect of Large-scale disturbance (LSD) on regulating tree fraction over the savanna areas is also investigated. The parameter for LSD is tuned to generate a reasonable tree cover distribution there.

3.1.1 Quasi-equilibrium simulation

DGVMs requires initial conditions for a number of state variables. DGVMs normally take 50-1000 years' simulation under specified meteorological forcing to reach this steady-state (Bonan and Levis, 2006; Zeng et al., 2008). Since our purpose was to generate initial condition for the decadal simulations, we applied a shortcut to reach the quasi-equilibrium coexistence of PFTs under the climatological forcing. We started the model from a SSiB 1-degree dominant vegetation map (Xue et al., 2004), with 100% occupation of the dominant PFT and zero for other PFTs at each grid point. The 1948-2007 averaged meteorological forcing along with 1948 CO_2 concentration was used to drive the SSiB4/TRIFFID for 100 years. SSiB4/TRIFFID is a water, energy, and carbon balanced model. Plants expansion, and biotic properties

such as vegetation height and LAI are constrained by carbon allocation. FRAC links the carbon accumulation within plants and intra-species competition via a system of the Lotka-Volterra equations (Cox, 2001). In the early first ten years of the simulation, most PFTs' FRACs change rapidly, but then take decades to reach a steady state (**Figure 1**). To qualify the steady state, we define quasi-equilibrium status as occurring when the rate of change of vegetation fraction is less than 2% of the mean vegetation fraction, over the last ten years of simulation. The result shows 100-year spin-up time is sufficient for our model. Overall, in the tropical areas (23.5°S~23.5°N), C4 plants and evergreen broadleaf trees are of mixed dominance and coexistent with C3 grasses, shrubs, and deciduous broadleaf trees. The subtropical areas (23.5°~35° in both hemispheres) are dominated by C3 grasses, C4 plants, and shrubs with similar occupation for each (~18%), whereas 40% of the subtropical areas are occupied by bare land. Needle leaf trees, C3 grasses, shrubs, and deciduous broadleaf trees are mix dominant the temperate zones (35°~66.5°, particularly in North Hemispheres). Over the polar areas (66.5°~90° in both hemispheres), shrubs and tundra are of mixed dominance (**Figure 1**).

3.1.2 Effect of large-scale disturbance

large-scale disturbance such as fire, and insect outbreaks alter physical structure and/or arrangement of biotic elements with great effect. TRIFFID introduce only a global uniform and PFT depended parameter to represent the rate of vegetation loss caused by LSD (units: yr^{-1}). The preliminary quasi-equilibrium run shows that under this approach, trees extended into the South American and African savanna areas (**Figure 2a**), where the climate acting alone would seem to favour tree growth (Bond et al., 2005). However, major ecological disturbances vary spatially and temporally (Giglio et al., 2006). We raised the LSD coefficient (largely representing fire at this scale) from 0.004 to 0.04 (yr^{-1}) for tree PFTs that coexist with C3 grasses and C4 plants. With the updated setting, the SSiB4/TRIFFID produced reasonable dominant tree coverage over the tropical rainforest areas (**Figure 2b**) in comparison with the GLC2000 dataset (**Figure 2c**). The global PFT distributions in the equilibrium run are close to the results using the real meteorological forcing.

3.2 Model evaluation of simulated vegetation distribution, LAI and GPP

Using initial conditions derived from the equilibrium run for both biotic and abiotic variables such as FRAC, LAI, vegetation height, soil moisture, and temperature, the model is then driven with the historical meteorological forcing and yearly updating atmospheric CO_2 concentration from 1948 to 2007. In this section, the global (hereafter referring to the regions of 180°W to 180°E, 60°S to 75°N) distributions of the simulated FRAC, LAI, and GPP are compared to the observation-based datasets to ensure SSiB4/TRIFFID generates reasonable spatial pattern and temporal variability of those variables, which provides a base for further assessment of the impact of external drivers on some surface variables.

3.2.1 Vegetation spatial distribution

Satellite-derived products are used to assess the model-simulated mean FRAC averaged over last ten-year (**Figure 2**). Overall, the model simulated vegetated land cover of 79.6% of the global land surface, less than GLC2000 estimation, 80.8%, and higher than the MODIS estimation, 79.3% (**Figure S1**). There is no human activity included in the model simulation, as such an agricultural category is not included. Therefore, in the following vegetation coverage comparison with the GLC products, Simulated PFT coverage in the grid boxes with agriculture is reduced based on the GLC agriculture fraction. On this basis, the total simulated tree cover (the sum of evergreen broadleaf trees, deciduous broadleaf trees, and needle leaf trees) is 28.8%, close to 29.8% in GLC2000. The evergreen broadleaf trees in the Amazon, Central Africa, and Southeast Asia, deciduous broadleaf trees in southeast North America, and needle leaf trees in the high-mid latitudes of North America and Eurasia are reasonably predicted. The SSiB4/TRIFFID simulates 12.7% C3 grass occupation, which is slightly higher than 11.9% in the GLC2000, with reasonably simulation in the mid-latitudes in both hemispheres such as the central U.S., Eurasian Steppes, South America, South and East Africa, and East Australia. The model simulates 10.1% natural C4 plants, compared to 7.9% in the GLC2000. The discrepancy could be partially attributed to the absence of C4 plants in some GLC2000 regional maps (such as Southeast Asia). The global GLC2000 map is assembled from these regional maps. In fact, a satellite-based physiological model simulation estimated 13.9% of C4 plants coverage with no agriculture category (Still et al., 2003). In the

SSiB4/TRIFFID prediction without excluding agricultural land, the C4 plants cover 13.5%, close to Still et al's estimation. C4 plants are primarily located in South American and African savanna areas, the Indian Subcontinent, Southeast Asia, the southeast U.S., and northern Australia. The model simulates 15.9% shrubs and tundra occupation, which is close to 16.7% in the GLC2000, with shrubs primarily located in the semi-arid areas in both hemispheres and the pan-arctic area, while tundra is located in the pan-arctic area and Tibetan Plateau (**Figure 3** and also see vegetation fractional distribution in **Figure S2**).

3.2.2 Leaf area index

This section discusses the spatial and temporal correlations between the simulations and observations and compares with other model results. Since other published studies on this subject have not excluded agricultural areas when evaluating LAI and GPP simulation, to make our results comparable with others, the agricultural areas are not subtracted. In fact, the difference between the results with and without the exclusion of agriculture area for our results are less than 0.01.

SSiB4/TRIFFID produces a similar global LAI pattern compared to both the GIMMS and GLASS products, confirmed by global spatial correlation coefficients of 0.86 (GIMMS, $p<0.05$) and 0.87 (GLASS, $p<0.05$), and above 0.74 ($P<0.05$) against both observations over the Northern Hemisphere (**Figure 4**). Previous studies reported spatial correlation coefficients between models and GIMSS-LAI over the globe/Northern Hemisphere in the range of 0.44-0.77/0.21-0.61 (Murray-Tortarolo et al., 2013; Mahowald et al., 2015). The latter study reported that in general DGVMs tended to overestimate global average LAI by 0.69±0.44 units calculated based on the table in Mahowald et al. (2015). The SSiB4/TRIFFID produces ~0.95 units higher global averaged LAI than the satellite-derived data. The absence of nitrogen limitation in the model could contribute to the overestimation.

3.2.3 Gross primary product

The spatial correlation coefficient between model and FLUXNET-MTE GPP is 0.93 ($P<0.05$) (**Figure 5**). Anav et al. (2015) reported less than 0.8 correlation against FLUXNET-MTE GPP for multi-model comparison. Over the globe, SSiB4/TRIFFID simulates 151 PgC/yr, greater than the FLUXNET-

MTE average of 122 PgC/yr. However, our simulation was still within the range of 130-169 PgC/yr reported by Anav et al. (2015) and 111-151 PgC/yr reported by Piao et al. (2013). In addition to our model's deficiencies (such as lack of N-limitation), the lack of CO_2 fertilization during the MTE model training may have contributed to an underestimation in the FLUXNET-MTE GPP.

3.3 Simulated vegetation temporal variability

3.3.1 Vegetation temporal variability during 1982-2007 and its comparison to observation-based data

Model performance in predicting temporal variability has been less evaluated in previous studies on ecosystem trend detection and attribution (Ichii et al., 2013; Piao et al., 2013; Zhang et al., 2015). However, performance in estimating LAI and GPP trends and variability has been found to vary among models (Murray-Tortarolo et al., 2013; Piao et al., 2013; Anav et al., 2015; Zhu et al., 2017). To better assess model performance in this regard, we select 13 sub-regions associated with different regional climate and land cover conditions (**Table 2)**. Although the MTE excludes CO_2 fertilization during its model training, FLUXNET-MTE GPP still incorporates variability at different scales associated with climate variability and is widely used by the community for model evaluation. Both annual LAI and GPP correlation coefficients are calculated over the period of 1982-2007.

Globally, the correlations for annual mean LAI between the SSiB4/TRIFFID and the satellite-based products are 0.58 ($P<0.05$) for GIMMS and 0.64 ($P<0.05$) for GLASS. The correlation for annual GPP is 0.59 ($P<0.05$) between the SSiB4/TRIFFID and FLUXNET-MTE GPP. Regionally, LAI correlations over West Africa are 0.79 ($P<0.05$) with GIMMS and 0.77 ($P<0.05$) with GLASS **(Figure 6**), and GPP correlation is 0.80 ($P<0.05$) with FLUXNET-MTE GPP in that region. For other semi-arid areas in western North America, South American savanna areas, and East Africa, the simulated LAI significantly matches at least one of the two reference datasets with correlation in the range of 0.46-0.58 ($P<0.05$). The simulated GPP correlations with FLUXNET-MTE GPP are in the range of 0.63-0.70 ($P<0.05$). The LAI over the forested areas are better correlated to GLASS LAI, while GPP are only significantly corrected to FLUXNET-MTE GPP over the boreal forests. Over the cold regions (subarctic

and Tibetan Plateau), the SSiB4/TRIFFID matches the reference data in a varying range of 0.46-0.74 ($P<0.05$) for LAI and 0.49-0.72 ($P<0.05$) for GPP.

Distinct decadal variabilities are identified in most sub-regions. For instance, trends reversal sign in West Africa (from negative to positive) and western North America (from positive to negative) during the 1980s (**Figure 6**). Areas with enhancement in trends slopes, such as the subarctic after the climate regime shift in the 1980s, will be discussed in detail in the next section.

Generally, SSiB4/TRIFFID simulates reasonable predictions of terrestrial ecosystem climatology and variability compared to the observation-based datasets (**Table 2**). Compared to other DGVMs, SSiB4/TRIFFID shows above average performance in reproducing the spatial distribution, but with certain bias in absolute numbers. In particular, SSiB4/TRIFFID captures the ecosystem temporal variabilities over different regions across the world, which provides a basis for pursuing the ecosystem trends detection and attribution study presented in the next section.

3.3.2 Three major types of vegetation trend change since the 1950s

The climate regime shifted abruptly during the 1980s, giving rise to changing in ecosystem trends in many parts of the world. Here we compare trends of FRAC, LAI, and GPP over two periods: 1958-1982 and 1982-2007. The model performance for the second period, for which satellite observations are available, is evaluated in Section 3.3.1. Spatial patterns of the trends are shown in **Figure 7**.

At the global scale, significant vegetation trends are only found in the simulations after the 1980s. During this period, FRAC increases at the rate of 0.032/yr. LAI has a positive trend of 0.0029/yr, which matches very well to GIMMS' results (0.0029/yr). GPP has a positive trend of 2.22 $gC/m^2/yr^2$, within the range of 1.60-4.69 $gC/m^2/yr^2$ for GPP over similar periods (Anav et al., 2015; Yue et al., 2015). In contrast to LAI and GPP, there are relatively few areas with a significant simulated FRAC trend (**Figure 7**).

For the global land surface, over 40.2% has a significant LAI trend since 1958 through 2007, and over 48.1% has a significant GPP trend. In response to the climate regime shift during the 1980s, the terrestrial ecosystem has three major trend changes in different parts of the world after the 1980s (**Table 4**). 1) There is trend sign reversal from negative to positive in the East Asian monsoon area, West Africa,

Central Asia, and Eastern US, over 14.2% (LAI) and 11.4% (GPP) of the land surface. In particular, West Africa experiences the largest vegetation deterioration in the world before the 1980s, associated with LAI and GPP reductions of 0.0258/yr and 18.54 $gC/m^2/yr^2$, respectively - approximately 10 times the trends of the global average. After the 1980s, recovery is simulated at the rate of 0.0137/yr and 8.02 $gC/m^2/yr^2$ for LAI and GPP, respectively. 2) Trend sign reversal from positive to negative is found in western North America, South America savanna and East Africa, which accounted for 2.9% (LAI) and 2.7% (GPP) of the land surface. 3) There are consistent positive trends but substantially enhanced by at least 50% of prior period trends after the 1980s, which are found in Equatorial rainforest areas, boreal forest areas, South Africa, North Australia, subarctic areas, and the Tibetan Plateau, representing over 11.7% (LAI) and 19.3% (GPP) of the land surface. There are also areas with consistent positive trends but no substantial change during the entire period or other types of trend change over much smaller areas. The first three major trend changes as described above will be discussed in the following sections.

3.4 Attribution of three environmental drivers on ecosystem trends

3.4.1 Global overview of three simulated environmental drivers' effects on the ecosystem trends

Sensitivity experiments were conducted to isolate the contributions of elevated atmospheric CO_2 concentration, global warming, and climate variability. The differences between the control experiment and Fixed-CO_2 shows that eCO_2 stimulated vegetation growth mainly in the Equatorial areas and eastern North America, Western Europe, and Eastern China in the mid-latitudes. Substantially enhanced positive trends are found after the 1980s for both LAI and GPP over those areas (**Figure 8**). eCO_2 promoted rainforest LAI increase only after the 1980s; however, its effect on GPP appeared during the entire period. GPP is directly linked to CO_2 through the photosynthesis process, while LAI, in addition to the photosynthesis process, is also affected by respiration and carbon allocation in plants, which are influenced by both climate and eCO_2 (O'Sullivan O et al., 2017).

The differences between the control experiment and Detrend-Temp shows that global warming has minor effects on the trends of LAI and GPP before the 1980s (**Figure 9**). After the 1980s, the rapidly enhanced warming contributes positive LAI trends at high latitudes, while the GPP change seems less

substantial. Meanwhile, there are negative trends due to heat stress in low latitudes, particularly in the semi-arid regions such as South American savanna, East Africa, and central Asia.

The differences between the control experiment and Fixed-CO_2 and Detrend-Temp show the CV effect, which has complex influences on the ecosystem. The CV in this study includes contribution of changes in surface pressure, precipitation, surface wind speed, downward longwave and shortwave radiations, surface humidity, along with temperature that excludes the global warming trend. Precipitation is however found to play a dominant role. The correlation coefficients between the annual mean CV effect on LAI and GPP and annual mean precipitation at the grid points with significant CV effect are greater than 0.60 ($P<0.05$). Overall, the CV effect alone can explain the total FRAC trends in the control experiment (**Figure 10**). Before the 1980s, CV causes LAI decrease in East Asian monsoon areas, eastern North America, West Africa, Western Europe, Central Asia, Siberia, and eastern Australia. The GPP also decreases in these areas except for eastern North America, Western Europe, and Siberia. In contrast, the CV effect before the 1980s leads LAI and GPP increase in the Tibetan Plateau and South Asia, western North America, South American savanna areas, East and South Africa, and northern Australia. Due to the climate regime shift, CV has produced the opposite sign to the trends of LAI and GPP in East Asian monsoon areas, Central Asia, West Africa, North America, South American savanna areas, and East Africa. In some areas, such as South Africa and northern Australia, persistent precipitation increase/decrease leads to sustained positive/negative trends from the 1950s.

Overall, after the 1980s, the effects of eCO_2 and global warming have been generally enhanced; but the CV effect has exhibited distinctly different regional features before/after the 1980s over many regions in the world. The enhanced or opposite contribution of the primary driver and the changes in their relative importance on the ecosystem trends occur during the 1980s, result in different ecosystem responses in many regions across the world.

3.4.2 Dominant factor in influencing trend reversal from negative to positive in West Africa and East Asia

CV is found to be the dominant driver of the ecosystem trends in West Africa, explaining most of the LAI and GPP trends and trend changes (Figure 11a). Before the 1980s, CV causes C4 plants' LAI, GPP, and FRAC over the region to decrease, followed by shrubs, whereas eCO_2 caused C3 grasses' LAI and GPP

to slightly increase. Global warming shows little effect during the entire period from 1958-2007. The ecosystem trends in West Africa reverses from decrease to increase when the precipitation trend changes to increase after the 1980s, with the major increase in C3 grasses and shrubs over the region. A previous study using satellite data also showed recent West Africa greening is highly correlated to the precipitation increase (Herrmann et al., 2005). eCO_2 plays a role in increasing C3 grasses coverage since the 1950s. However, the PFT competition outcomes reduce the C4 plant coverage over the region, mainly after the 1980s when eCO_2 has a large impact. As such, the change in regional FRAC overall within West Africa is not significant and has been compromised by positive and negative contributions of the individual PFTs after the 1980s.

Regional average trends reverse in the East Asian monsoon area because CV and eCO_2 dominate LAI and GPP trends, before and after the 1980s, respectively. Their combined effects cause trend reversal in the East Asian monsoon areas. CV contributes decreasing trends of LAI and GPP before the 1980s, but with minor effects after the 1980s. While eCO_2 dominates the PFT LAI and GPP trends since the 1950s, which caused significant increase in C3 grasses and trees but significant decrease in C4 plants (**Figure 11b**). Meanwhile, enhanced global warming after the 1980s stimulates C4 plant growth, but this effect is compromised by its detrimental effect on C3 grasses after the 1980s. Overall, CV and eCO_2 relative contribution change during the 1980s dominate the negative to positive trends shift in this area.

3.4.3 Dominant factor in influencing trend reversal from positive to negative in western North America

The eCO_2 effect persistently causes LAI, GPP, and FRAC increase since the 1950s, while global warming reduced both LAI and GPP only after the 1980s. However, CV dominated the LAI and GPP trends and trends reversal in western North America by causing the dominant PFTs (C3 grasses and shrubs) to increase/decrease before/after the 1980s (**Figure 11c** and **Table 5**). The CV effect on FRAC change is more complex due to its different effects on LAI and GPP and FRAC expansion in C3 and shrub PFTs after the 1980s: both C3 and shrubs expand with LAI and GPP decrease. This discrepancy suggests that expansion might be coupled with carbon fixation less than with growth in the model. We conjecture that CV may promote vegetation expansion into some areas that are largely un-vegetated, but this requires further investigation.

3.4.4 Dominant factor in influencing the enhanced positive trend in rainforest, boreal forest, subarctic, and Tibetan Plateau

eCO_2 and CV have persistent positive impacts on tropical rainforest growth in terms of LAI and GPP since the 1950s (**Figure 11d**). eCO_2 dominates the LAI and GPP trends in both periods except for the LAI positive trend before the 1980s, which is dominated by CV. LAI trend enhancement after the 1980s is associated with increased CO_2 fertilization, while GPP trend enhancement is attributed to increase in both eCO_2 and CV effects. The importance of CO_2 and CV impacts on the rainforests is confirmed by previous analyses on the trends of LAI and NDVI (Hilker et al., 2014; Zhu et al., 2016).

eCO_2 and global warming increase LAI and GPP in North American boreal forest areas since the 1950s and cause significant positive trends over the Eurasian boreal forest area after the 1980s (**Figure 11e**). However, due to CV-induced negative effects on tree LAI, no significant trend is found in regional average LAI in boreal areas before the 1980s. The LAI and GPP trend enhancement in the boreal forest areas can be attributed to the enhanced eCO_2 and global warming effects, accompanied by reduced CV negative effects after the 1980s.

North American subarctic areas have enhanced LAI and GPP positive trends after the 1980s, which were caused by the increase in eCO_2 and CV positive effects, while all three environmental drivers have effects on LAI and GPP positive trends in the Eurasian subarctic (**Figure 11f**). Meanwhile, remarkable FRAC changes are found since the 1950s. Our simulation suggests that global warming continually favorited shrub invasion into tundra biomes, except in the Eurasian subarctic before the 1980s. After the 1980s, this shrubification is enhanced due to increase in the warming effect. In contrast, eCO_2 has promoted tundra expansion and shrub decline over subarctic areas since the 1950s, which mitigates the shrubification. Meanwhile, CV plays a role to help tree and C3 grass expansion into subarctic areas, and also alters the shrub and tundra competition.

Over the Tibetan Plateau (**Figure 11g**), CV dominates the positive LAI and GPP trends since the 1950s, excepted in the case of the GPP increase before the 1980s which is dominated by eCO_2. The positive trend enhancements for LAI and GPP after the 1980s are caused by the impact of both eCO_2 and CV. Furthermore, our simulation also suggests that CV favours C3 grasses but harms tundra biome expansion. However, eCO_2 has the opposite effects on those PFTs, in contrast to the CV's.

4. Discussion

The spatial distribution of the dominant PFT is closely related to large-scale climate (MacDonald, 2002) and DGVMs are designed to reproduce the observed ecosystem/climate relationship. There are diverse performances in reproducing the spatial distribution and temporal variability of the ecosystems (Murray-Tortarolo et al., 2013; Piao et al., 2013; Anav et al., 2015; Zhu et al., 2017), which resulted in large discrepancies between models in identifying attributed dominant drivers of changes (Beer et al., 2010; Huntzinger et al., 2017). It is therefore important to validate the model performance in reproducing the observed ecosystem variability and spatial distribution first before using DGVMs for attribution studies. As a matter of fact, it is challenge for DGVMs to reproduce PFT coexistence, particularly for the smaller PFTs in semi-humid and semi-arid areas as they are fragile and sensitive to climate and vulnerable to competition (Fu et al., 2006). Because of that difficulty, Zeng et al. (2008) had to introduce a specific sub-model to grow temperate shrubs in the spaces unoccupied by trees and grasses. The SSiB4/TRIFFID allows smaller fractions of PFTs to co-exist with full competition with other PFTs (Cox, 2001). After modifying the competition coefficients in the Lotka-Volterra equation (Zhang et al., 2015) and updating large-scale disturbance parameters, it produces reasonable global distribution of temperate shrubs and high-latitudes tundra (**Figure 3**). During the validation process, some parameters in the SSiB4/TRIFFID have also been calibrated (Zhang et al., 2015).

With all these efforts, the SSiB4/TRIFFID produced LAI and GPP show higher temporal correlation with observation compared to the start-of-art offline models in the TRENDY intercomparison project (Piao et al., 2013; Sitch et al., 2015; Zhu et al., 2016). The improvement may mainly be due to better capturing of the interannual variability by the SSiB4/TRIFFID in semi-arid areas, which has been considered as dominating global interannual variability (Poulter et al., 2014; Ahlstrom et al., 2015). Meanwhile, both simulated LAI and GPP are also well correlated with reference data over the Northern Hemisphere boreal forests. Our evaluation is based on satellite-based products, which are the only sources providing global distribution at long term. Although these products showed a general consistency among them, large relative uncertainties were identified over some regions (Jiang et al., 2017), which contribute to large discrepancy of interannual correlations when the simulated LAI compared to GIMMS and GLASS LAIs (**Figure 6**). It should be pointed out that the GPP simulation over the rainforests exhibit

inconsistency with the FLUXNET-MTE GPP. We consider that the missing CO_2 fertilization in FLUXNET-MTE GPP could be a predominant limitation to its GPP there. By and large, the SSiB4/TRIFID's performance suggest this model is proper to be applied for the attribution study.

The SSiB4/TRIFFID simulates increased LAI and GPP after the 1980s (**Figure 8**), which is confirmed by observation and the TRENDY models' simulation (Anav et al., 2013 for GPP; Piao et al., 2013 and Zhu et al., 2016 for LAI). These increases are considered to responding to elevated atmospheric CO_2 concentrations and warming surface temperature in high-latitudes (Zhu et al., 2016). Some areas with decrease LAI and GPP are due to decrease in precipitation and/or increase in stress due to warming temperature in low-latitudes (Anav et al., 2013; Zhu et al., 2016). Our study, however, further estimate large-scale trends in all three aspects, i.e. carbon fixation (GPP), vegetation growth (LAI), as well as expansion, rather than focus only on one aspect, such as LAI trend in Zhu et al. (2016). Our results also reveal different LAI and GPP response to the environmental changes (**Figure 8-10**), indicating LAI and GPP are involved in different process as discussed in O'Sullivan O et al. (2017). The results suggest that GPP is more directly linked to atmospheric CO_2 (**Figure 8**).

In SSiB4/TRIFFID, net CO_2 assimilation is proportional to the gradient of atmosphere and leaf CO_2 concentration (Zhan et al., 2013, also see supplement). Hence the elevated atmospheric CO_2 concentration leads to increase in GPP. While LAI in TRIFFID is related to carbon allocation and competition between PFTs. As such, LAI is not only affected by the atmospheric carbon concentration, but also other processes, such as phenological processes and the percentage collocated carbon for growth. Therefore, GPP is more sensitive to the change in atmospheric carbon concentration compared to LAI. Integrated analysis and observation with multiple variables, such as LAI and GPP, are required to improve the understanding of vegetation biochemical process and climate effect on ecosystem changes.

The competition between PFTs within a grid box contributes to the ecosystem trend discussed above. Our analysis with grid point has shown intensive interactions between PFTs. For instance, shrubs are found to expand into tundra ecosystems (**Figure 11f**), which is linked to climate change (Myers-Smith et al., 2015), particularly to global warming (Tape et al., 2006; Elmendorf et al., 2012) and precipitation (Martin et al., 2017). The response to eCO_2 of a particular PFT not only depends on its own physiological and morphological characteristics, but is also determined by the interactions that arise with other PFTs,

competing for the same resources (**Figure 11a**). Field experiments reported that the differential growth and competitiveness responses of C3 and C4 plants to eCO_2 is complex and under debate (Leakey et al., 2009; Lee 2011; Miri et al., 2012). In this paper, we have discussed the competition between C3 and C4, and its contribution to the trend change. It seems under the elevated atmospheric CO_2 concentration scenario C3 grasses show enhanced competitive ability over C4 plant at regional scale (**Figure 11b**). Different responses of the co-exist PFTs to the climate regime shift either enhance or mitigate the environmental drivers' contribution at grid averaged scale.

Furthermore, our results show that the boundary between Sahara and Sahel has experienced significant variation since the 1950s. Based on the observed precipitation data and the precipitation/NDVI correlation, Thomas and Nigam (2018) suggested a Sahara Desert expansion since the 1950s. Our results are in an agreement at large with the Thomas and Nigam's study (2018) but also with substantial differences in the rate at two different climate regimes. A comprehensive discussion on this issue is out of scope of this paper and will be addressed in a separate paper.

5. Conclusion

This work employs a biophysical-dynamic vegetation model (SSiB4/TRIFFID) to explore the responses of the terrestrial ecosystem to climate variability, global warming, and elevated atmospheric CO_2 concentration during 1948-2007. The SSiB4/TRIFFID is evaluated by available satellite data in simulating the land surface carbon fixation, and plant growth and competition. We have shown that the SSiB4/TRIFFID model can simulate the vegetation and temporal variability for the period of 1982-2007. A series of sensitivity experiments are then conducted to detect the ecosystem trends and attribute the trends to elevated atmospheric CO_2 concentration (eCO_2), global warming, and climate variability (CV).

The effects of the external drivers on the ecosystem trends manifest distinct spatial and temporal characteristics. For the global land surface, over 40.2% has a significant LAI trend and over 48.1% had a significant GPP trend since the 1958 through 2007. In responding to the climate regime shift during the 1980s, the terrestrial ecosystem has three major changes in different parts of the world after the 1980s. Over 14.2% (LAI) and 11.4% (GPP) of the land surface, primarily located in East Asian monsoon area, West Africa, Central Asia, and Eastern US, had trend sign reversal from negative to positive. In contrast,

trend reversal from positive to negative is found in western North America, South America savanna and East Africa, which accounted for 2.9% (LAI) and 2.7% (GPP) of the land surface. Meanwhile, there are consistent positive trends substantially enhanced in Equatorial rainforest areas, boreal forest areas, South Africa, North Australia, subarctic areas, and the Tibetan Plateau, representing over 11.7% (LAI) and 19.3% (GPP) of the land surface, respectively.

In general, the major types of trend change are attributed to the changes in relative contributions of environmental drivers, and, consequently, the changes in the dominate driver; or changes in the dominant driver's "direction" in its effect (enhancing or suppression) on ecosystem. The eCO_2 stimulates vegetation growth through fertilization effects mainly in the Equatorial areas, as well as eastern North America, Western Europe, and Eastern China in the mid-latitudes. The rapidly enhanced global warming after the 1980s contributes positive LAI trends at high latitude, while the GPP change seems less substantial. Meanwhile, there are negative trends in LAI and GPP due to the heat stress in low latitudes. CV dominates the variability of FRAC, LAI and GPP in the semi-humid and semi-arid areas. The overall effects on the ecosystem are the integrated contribution of all environmental drivers.

Data availability

SSiB4/TRIFFID simulated vegetation fraction, LAI and GPP are available at https://ucla.box.com/v/ssib4-offline

Acknowledgements

This work was supported by NSF Grant AGS-1419526.

Competing interests

The authors declare that they have no conflict of interest.

References

Ahlbeck, J. R.: Comment on "Variations in northern vegetation activity inferred from satellite data of vegetation index during 1981-1999" by L. Zhou et al, Journal of Geophysical Research: Atmospheres, 107, 2002.

Ahlstrom, A., Raupach, M. R., Schurgers, G., Smith, B., Arneth, A., Jung, M., Reichstein, M., Canadell, J. G., Friedlingstein, P., Jain, A. K., Kato, E., Poulter, B., Sitch, S., Stocker, B. D., Viovy, N., Wang, Y. P., Wiltshire, A., Zaehle, S., and Zeng, N.: Carbon cycle. The dominant role of semi-arid ecosystems in the trend and variability of the land CO(2) sink, Science, 348, 895-899, 2015.

Anav, A., Friedlingstein, P., Beer, C., Ciais, P., Harper, A., Jones, C., Murray-Tortarolo, G., Papale, D., Parazoo, N. C., Peylin, P., Piao, S. L., Sitch, S., Viovy, N., Wiltshire, A., and Zhao, M. S.: Spatiotemporal patterns of terrestrial gross primary production: A review, Reviews of Geophysics, 53, 785-818, 2015.

Ballantyne, A. P., Alden, C. B., Miller, J. B., and Tans, P. P.: Increase in observed net carbon dioxide uptake by land and oceans during the past 50 years - ProQuest, Nature, 2012.

Bartalev, S. A., Belward, A. S., Erchov, D. V., and Isaev, A. S.: A new SPOT4-VEGETATION derived land cover map of Northern Eurasia, International Journal of Remote Sensing, 24, 1977-1982, 2003.

Bartholome, E., Belward, A. S., Achard, F., Bartalev, S., Carmona-Moreno, C., Eva, H., Fritz, S., Gregoire, J. M., Mayaux, P., and Stibig, H. J.: GLC 2000: Global Land Cover mapping for the year 2000, Project status, November, 2002.

Beer, C., Reichstein, M., Tomelleri, E., Ciais, P., Jung, M., Carvalhais, N., Rodenbeck, C., Arain, M. A., Baldocchi, D., Bonan, G. B., Bondeau, A., Cescatti, A., Lasslop, G., Lindroth, A., Lomas, M., Luyssaert, S., Margolis, H., Oleson, K. W., Roupsard, O., Veenendaal, E., Viovy, N., Williams, C., Woodward, F. I., and Papale, D.: Terrestrial gross carbon dioxide uptake: global distribution and covariation with climate, Science, 329, 834-838, 2010.

Bonan, G. B., Levis, S., Sitch, S., Vertenstein, M., and Oleson, K. W.: A dynamic global vegetation model for use with climate models, 2002.

Bonan, G. B., and Levis, S.: Evaluating aspects of the community land and atmosphere models (CLM3 and CAM3) using a Dynamic Global Vegetation Model, Journal of Climate, 19, 2290-2301, 2006.

Bond, W. J., Woodward, F. I., and Midgley, G. F.: The global distribution of ecosystems in a world without fire, New Phytol, 165, 525-537, 10.1111/j.1469-8137.2004.01252.x, 2005.

Claussen, M., and Gayler, V.: The greening of the Sahara during the mid-Holocene: results of an interactive atmosphere-biome model, Global Ecology and Biogeography Letters, 6, 369-377, 1997.

Collatz, G. J., Ball, J. T., Grivet, C., and Berry, J. A.: Physiological and Environmental-Regulation of Stomatal Conductance, Photosynthesis and Transpiration - a Model That Includes a Laminar Boundary-Layer, Agricultural and Forest Meteorology, 54, 107-136, 1991.

Collatz, G. J., Ribas-Carbo, M., and Berry, J. A.: Coupled Photosynthesis-Stomatal Conductance Model for Leaves of C4 Plants, Australian Journal of Plant Physiology, 19, 519-538, 1992.

Cox, P., Betts, R. A., Jones, C. D., Spall, S. A., and Totterdell, I. J.: Acceleration of global warming due to carbon-cycle feedbacks in a coupled climate model, Nature, 408, 184-187, 2000.

Cox, P.: Description of the "TRIFFID" Dynamic Global Vegetation Model, Hadley Centre technical note, 24, 1-16, 2001.

Cramer, W., Bondeau, A., Woodward, F. I., Prentice, I. C., Betts, R. A., Brovkin, V., Cox, P. M., Fisher, V., Foley, J. A., Friend, A. D., Kucharik, C., Lomas, M. R., Ramankutty, N., Sitch, S., Smith, B., White, A., and Young-Molling, C.: Global response of terrestrial ecosystem structure and function to CO2 and climate change: results from six dynamic global vegetation models, Global Change Biology, 7, 357-373, 2001.

Devaraju, N., Bala, G., Caldeira, K., and Nemani, R.: A model based investigation of the relative importance of CO2-fertilization, climate warming, nitrogen deposition and land use change on the global terrestrial carbon uptake in the historical period, Climate Dynamics, 47, 173-190, 2016.

Donohue, R. J., McVicar, T. R., and Roderick, M. L.: Climate-related trends in Australian vegetation cover as inferred from satellite observations, 1981-2006, Global Change Biology, 15, 1025-1039, 2009.

Dorman, J. L., and Sellers, P. J.: A Global Climatology of Albedo, Roughness Length and Stomatal-Resistance for Atmospheric General-Circulation Models as Represented by the Simple Biosphere Model (Sib), Journal of Applied Meteorology, 28, 833-855, 1989.

Elmendorf, S. C., Henry, G. H. R., Hollister, R. D., Bjork, R. G., Boulanger-Lapointe, N., Cooper, E. J., Cornelissen, J. H. C., Day, T. A., Dorrepaal, E., Elumeeva, T. G., Gill, M., Gould, W. A., Harte, J., Hik, D. S., Hofgaard, A., Johnson, D. R., Johnstone, J. F., Jonsdottir, I. S., Jorgenson, J. C., Klanderud, K., Klein, J. A., Koh, S., Kudo, G., Lara, M., Levesque, E., Magnusson, B., May, J. L., Mercado-Diaz, J. A., Michelsen, A., Molau, U., Myers-Smith, I. H., Oberbauer, S. F., Onipchenko, V. G., Rixen, C., Schmidt, N. M., Shaver, G. R., Spasojevic, M. J., Porhallsdottir, P. E., Tolvanen, A., Troxler, T., Tweedie, C. E., Villareal, S., Wahren, C. H., Walker, X., Webber, P. J., Welker, J. M., and Wipf, S.: Plot-scale evidence of tundra vegetation change and links to recent summer warming, Nature Climate Change, 2, 453-457, 2012.

Epstein, H. E., Raynolds, M. K., Walker, D. A., Bhatt, U. S., Tucker, C. J., and Pinzon, J. E.: Dynamics of aboveground phytomass of the circumpolar Arctic tundra during the past three decades, Environmental Research Letters, 7, 015506, 2012.

Friedl, M. A., Sulla-Menashe, D., Tan, B., Schneider, A., Ramankutty, N., Sibley, A., and Huang, X. M.: MODIS Collection 5 global land cover: Algorithm refinements and characterization of new datasets, Remote Sensing of Environment, 114, 168-182, 2010.

Friedlingstein, P., Cox, P., Betts, R., Bopp, L., Von Bloh, W., Brovkin, V., Cadule, P., Doney, S., Eby, M., Fung, I., Bala, G., John, J., Jones, C., Joos, F., Kato, T., Kawamiya, M., Knorr, W., Lindsay, K., Matthews, H. D., Raddatz, T., Rayner, P., Reick, C., Roeckner, E., Schnitzler, K. G., Schnur, R., Strassmann, K., Weaver, A. J., Yoshikawa, C., and Zeng, N.: Climate-carbon cycle feedback analysis: Results from the (CMIP)-M-4 model intercomparison, Journal of Climate, 19, 3337-3353, 2006.

Fu, C., Yan, X. D., and Guo, W. D.: Aridification of northern china and adaptability of humanbeing: Use the concept of earth system science to solve global regional respondence and adaptability problems under demands of natio, Progress in Natural Science, 16, 1216-1223, 2006.

Garcia, R. A., Cabeza, M., Rahbek, C., and Araujo, M. B.: Multiple dimensions of climate change and their implications for biodiversity, Science, 344, 1247579, 10.1126/science.1247579, 2014.

Giglio, L., Csiszar, I. and Justice, C.O.,: Global distribution and seasonality of active fires as observed with the Terra and Aqua Moderate Resolution Imaging Spectroradiometer (MODIS) sensors. Journal of Geophysical Research: Biogeosciences, 111(G2), 2006

Gong, D., and Ho, C. H.: Shift in the summer rainfall over the Yangtze River valley in the late 1970s, Geophysical Research Letters, 29, 78-71-78-74, 2002.

Hare, S. R., and Mantua, N. J.: Empirical evidence for North Pacific regime shifts in 1977 and 1989, Progress in Oceanography, 47, 103-145, 2000.

Herrmann, S. M., Anyamba, A., and Tucker, C. J.: Recent trends in vegetation dynamics in the African Sahel and their relationship to climate, Global Environmental Change-Human and Policy Dimensions, 15, 394-404, 2005.

Hilker, T., Lyapustin, A. I., Tucker, C. J., Hall, F. G., Myneni, R. B., Wang, Y., Bi, J., Mendes de Moura, Y., and Sellers, P. J.: Vegetation dynamics and rainfall sensitivity of the Amazon, Proc Natl Acad Sci U S A, 111, 16041-16046, 2014.

Huntzinger, D. N., Michalak, A. M., Schwalm, C., Ciais, P., King, A. W., Fang, Y., Schaefer, K., Wei, Y., Cook, R. B., Fisher, J. B., Hayes, D., Huang, M., Ito, A., Jain, A. K., Lei, H., Lu, C., Maignan, F., Mao, J., Parazoo, N., Peng, S., Poulter, B., Ricciuto, D., Shi, X., Tian, H., Wang, W., Zeng, N., and Zhao, F.: Uncertainty in the response of terrestrial carbon sink to environmental drivers undermines carbon-climate feedback predictions, Sci Rep, 7, 4765, 2017.

Ichii, K., Kondo, M., Okabe, Y., Ueyama, M., Kobayashi, H., Lee, S. J., Saigusa, N., Zhu, Z. C., and Myneni, R. B.: Recent Changes in Terrestrial Gross Primary Productivity in Asia from 1982 to 2011, Remote Sensing, 5, 6043-6062, 2013.

Jiang, C., Ryu, Y., Fang, H., Myneni, R., Claverie, M., and Zhu, Z.: Inconsistencies of interannual variability and trends in long-term satellite leaf area index products, Glob Chang Biol, 23, 4133-4146, 2017.

Jung, M., Reichstein, M., and Bondeau, A.: Towards global empirical upscaling of FLUXNET eddy covariance observations: validation of a model tree ensemble approach using a biosphere model, Biogeosciences, 6, 2001-2013, 2009.

Jung, M., Reichstein, M., Margolis, H. A., Cescatti, A., Richardson, A. D., Arain, M. A., Arneth, A., Bernhofer, C., Bonal, D., Chen, J. Q., Gianelle, D., Gobron, N., Kiely, G., Kutsch, W., Lasslop, G., Law, B. E., Lindroth, A., Merbold, L., Montagnani, L., Moors, E. J., Papale, D., Sottocornola, M., Vaccari, F., and Williams, C.: Global patterns of land-atmosphere fluxes of carbon dioxide, latent heat, and sensible heat derived from eddy covariance, satellite, and meteorological observations, Journal of Geophysical Research-Biogeosciences, 116, 16, 2011.

Krinner, G., Viovy, N., de Noblet-Ducoudré, N., Ogée, J., Polcher, J., Friedlingstein, P., Ciais, P., Sitch, S., and Prentice, I. C.: A dynamic global vegetation model for studies of the coupled atmosphere-biosphere system, Global Biogeochemical Cycles, 19, 2005.

Lawrence, D. M., Oleson, K. W., Flanner, M. G., Thornton, P. E., Swenson, S. C., Lawrence, P. J., Zeng, X. B., Yang, Z. L., Levis, S., Sakaguchi, K., Bonan, G. B., and Slater, A. G.: Parameterization Improvements and Functional and Structural Advances in Version 4 of the Community Land Model, J Adv Model Earth Sy, 3, 2011.

Le Quéré, C., Andres, R. J., Boden, T., Conway, T., Houghton, R. A., House, J. I., Marland, G., Peters, G. P., van der Werf, G. R., Ahlström, A., Andrew, R. M., Bopp, L., Canadell, J. G., Ciais, P.,

Doney, S. C., Enright, C., Friedlingstein, P., Huntingford, C., Jain, A. K., Jourdain, C., Kato, E., Keeling, R. F., Klein Goldewijk, K., Levis, S., Levy, P., Lomas, M., Poulter, B., Raupach, M. R., Schwinger, J., Sitch, S., Stocker, B. D., Viovy, N., Zaehle, S., and Zeng, N.: The global carbon budget 1959–2011, Earth System Science Data, 5, 165-185, 2013.

Leakey, A. D. B., Ainsworth, E. A., Bernacchi, C. J., Rogers, A., Long, S. P., and Ort, D. R.: Elevated CO2 effects on plant carbon, nitrogen, and water relations: six important lessons from FACE, Journal of Experimental Botany, 60, 2859-2876, 2009.

Lee, J.-S.: Combined effect of elevated CO2 and temperature on the growth and phenology of two annual C3 and C4 weedy species, Agriculture, ecosystems & environment, 140, 484-491, 2011.

Liu, Z., Notaro, M., Kutzbach, J., and Liu, N.: Assessing global vegetation-climate feedbacks from observations, Journal of Climate, 19, 787-814, 2006.

Lo, T. T., and Hsu, H. H.: Change in the dominant decadal patterns and the late 1980s abrupt warming in the extratropical Northern Hemisphere, Atmospheric Science Letters, 11, 210-215, 2010.

Los, S. O.: Analysis of trends in fused AVHRR and MODIS NDVI data for 1982-2006: Indication for a CO2 fertilization effect in global vegetation, Global Biogeochemical Cycles, 27, 318-330, 2013.

Ma, H., Mechoso, C. R., Xue, Y., Xiao, H., Neelin, J. D., and Ji, X.: On the Connection between Continental-Scale Land Surface Processes and the Tropical Climate in a Coupled Ocean-Atmosphere-Land System, Journal of Climate, 26, 9006-9025, 2013.

MacDonald, G.: Biogeography: introduction to space, time and life, John Wiley and Sons, 2002.

Mahowald, N., Lo, F., Zheng, Y., Harrison, L., Funk, C., and Lombardozzi, D.: Leaf Area Index in Earth System Models: evaluation and projections, Earth System Dynamics Discussions, 6, 761-818, 2015.

Mao, J., Shi, X., Thornton, P. E., Hoffman, F. M., Zhu, Z., and Myneni, R. B.: Global latitudinal-asymmetric vegetation growth trends and their driving mechanisms: 1982–2009, Remote Sensing, 5, 1484-1497, 2013.

Martin, A. C., Jeffers, E. S., Petrokofsky, G., Myers-Smith, I., and Macias-Fauria, M.: Shrub growth and expansion in the Arctic tundra: an assessment of controlling factors using an evidence-based approach, Environmental Research Letters, 12, 085007, 2017.

McDowell, N. G., Coops, N. C., Beck, P. S., Chambers, J. Q., Gangodagamage, C., Hicke, J. A., Huang, C. Y., Kennedy, R., Krofcheck, D. J., Litvak, M., Meddens, A. J., Muss, J., Negron-Juarez, R., Peng, C., Schwantes, A. M., Swenson, J. J., Vernon, L. J., Williams, A. P., Xu, C., Zhao, M., Running, S. W., and Allen, C. D.: Global satellite monitoring of climate-induced vegetation disturbances, Trends Plant Sci, 20, 114-123, 10.1016/j.tplants.2014.10.008, 2015.

Miri, H. R., Rastegar, A., and Bagheri, A. R.: The impact of elevated CO2 on growth and competitiveness of C3 and C4 crops and weeds, European Journal of Experimental Biology, 2, 1144-1150, 2012.

Mod, H. K., and Luoto, M.: Arctic shrubification mediates the impacts of warming climate on changes to tundra vegetation, Environmental Research Letters, 11, 10, 2016.

Murray-Tortarolo, G., Anav, A., Friedlingstein, P., Sitch, S., Piao, S. L., Zhu, Z. C., Poulter, B., Zaehle, S., Ahlstrom, A., Lomas, M., Levis, S., Viovy, N., and Zeng, N.: Evaluation of Land Surface Models in Reproducing Satellite-Derived LAI over the High-Latitude Northern Hemisphere. Part I: Uncoupled DGVMs, Remote Sensing, 5, 4819-4838, 2013.

Myers-Smith, I. H., Elmendorf, S. C., Beck, P. S. A., Wilmking, M., Hallinger, M., Blok, D., Tape, K. D., Rayback, S. A., Macias-Fauria, M., Forbes, B. C., Speed, J. D. M., Boulanger-Lapointe, N., Rixen, C., Lévesque, E., Schmidt, N. M., Baittinger, C., Trant, A. J., Hermanutz, L., Collier, L. S., Dawes, M. A., Lantz, T. C., Weijers, S., Jørgensen, R. H., Buchwal, A., Buras, A., Naito, A. T., Ravolainen, V., Schaepman-Strub, G., Wheeler, J. A., Wipf, S., Guay, K. C., Hik, D. S., and Vellend, M.: Climate sensitivity of shrub growth across the tundra biome, Nature Climate Change, 5, 887-891, 2015.

Myneni, R. B., Keeling, C. D., Tucker, C. J., Asrar, G., and Nemani, R. R.: Increased plant growth in the northern high latitudes from 1981 to 1991, Nature, 386, 698-702, 1997.

Nemani, R. R., Keeling, C. D., Hashimoto, H., Jolly, W. M., Piper, S. C., Tucker, C. J., Myneni, R. B., and Running, S. W.: Climate-driven increases in global terrestrial net primary production from 1982 to 1999, Science, 300, 1560-1563, 2003.

O'Sullivan O, S., Heskel, M. A., Reich, P. B., Tjoelker, M. G., Weerasinghe, L. K., Penillard, A., Zhu, L., Egerton, J. J., Bloomfield, K. J., Creek, D., Bahar, N. H., Griffin, K. L., Hurry, V., Meir, P., Turnbull, M. H., and Atkin, O. K.: Thermal limits of leaf metabolism across biomes, Glob Chang Biol, 23, 209-223, 2017.

Piao, S., Fang, J., Liu, H., and Zhu, B.: NDVI-indicated decline in desertification in China in the past two decades, Geophysical Research Letters, 32, 289, 2005.

Piao, S., Wang, X., Ciais, P., Zhu, B., Wang, T., and Liu, J.: Changes in satellite-derived vegetation growth trend in temperate and boreal Eurasia from 1982 to 2006, Global Change Biology, 17, 3228-3239, 2011.

Piao, S., Sitch, S., Ciais, P., Friedlingstein, P., Peylin, P., Wang, X., Ahlstrom, A., Anav, A., Canadell, J. G., Cong, N., Huntingford, C., Jung, M., Levis, S., Levy, P. E., Li, J., Lin, X., Lomas, M. R., Lu, M., Luo, Y., Ma, Y., Myneni, R. B., Poulter, B., Sun, Z., Wang, T., Viovy, N., Zaehle, S., and Zeng, N.: Evaluation of terrestrial carbon cycle models for their response to climate variability and to CO2 trends, Glob Chang Biol, 19, 2117-2132, 10.1111/gcb.12187, 2013.

Piao, S., Yin, G., Tan, J., Cheng, L., Huang, M., Li, Y., Liu, R., Mao, J., Myneni, R. B., Peng, S., Poulter, B., Shi, X., Xiao, Z., Zeng, N., Zeng, Z., and Wang, Y.: Detection and attribution of vegetation greening trend in China over the last 30 years, Glob Chang Biol, 21, 1601-1609, 2015.

Poulter, B., Frank, D., Ciais, P., Myneni, R.B., Andela, N., Bi, J., Broquet, G., Canadell, J.G., Chevallier, F., Liu, Y.Y. and Running, S.W.: Contribution of semi-arid ecosystems to interannual variability of the global carbon cycle. Nature 509:600–603. 2014

Reid, P. C., Hari, R. E., Beaugrand, G., Livingstone, D. M., Marty, C., Straile, D., Barichivich, J., Goberville, E., Adrian, R., Aono, Y., Brown, R., Foster, J., Groisman, P., Helaouet, P., Hsu, H. H., Kirby, R., Knight, J., Kraberg, A., Li, J., Lo, T. T., Myneni, R. B., North, R. P., Pounds, J. A., Sparks, T., Stubi, R., Tian, Y., Wiltshire, K. H., Xiao, D., and Zhu, Z.: Global impacts of the 1980s regime shift, Glob Chang Biol, 22, 682-703, 2016.

Schimel, D., Stephens, B. B., and Fisher, J. B.: Effect of increasing CO2 on the terrestrial carbon cycle, Proc Natl Acad Sci U S A, 112, 436-441, 2015.

Sheffield, J., Goteti, G., and Wood, E. F.: Development of a 50-year high-resolution global dataset of meteorological forcings for land surface modeling, Journal of Climate, 19, 3088-3111, 2006.

Sitch, S., Smith, B., Prentice, I. C., Arneth, A., Bondeau, A., Cramer, W., Kaplan, J. O., Levis, S., Lucht, W., Sykes, M. T., Thonicke, K., and Venevsky, S.: Evaluation of ecosystem dynamics, plant geography and terrestrial carbon cycling in the LPJ dynamic global vegetation model, Global Change Biology, 9, 161-185, 2003.

Sitch, S., Friedlingstein, P., Gruber, N., Jones, S. D., Murray-Tortarolo, G., Ahlstrom, A., Doney, S. C., Graven, H., Heinze, C., Huntingford, C., Levis, S., Levy, P. E., Lomas, M., Poulter, B., Viovy, N., Zaehle, S., Zeng, N., Arneth, A., Bonan, G., Bopp, L., Canadell, J. G., Chevallier, F., Ciais, P., Ellis, R., Gloor, M., Peylin, P., Piao, S. L., Le Quere, C., Smith, B., Zhu, Z., and Myneni, R.: Recent trends and drivers of regional sources and sinks of carbon dioxide, Biogeosciences, 12, 653-679, 2015.

Slevin, D., Tett, S. F. B., Exbrayat, J. F., Bloom, A. A., and Williams, M.: Global evaluation of gross primary productivity in the JULES land surface model v3.4.1, Geoscientific Model Development, 10, 2651-2670, 2017.

Smith, B., Prentice, I. C., and Sykes, M. T.: Representation of vegetation dynamics in the modelling of terrestrial ecosystems: comparing two contrasting approaches within European climate space, Global Ecology and Biogeography, 10, 621-637, 2001.

Smith, W. K., Reed, S. C., Cleveland, C. C., Ballantyne, A. P., Anderegg, W. R., Wieder, W. R., Liu, Y. Y., and Running, S. W.: Large divergence of satellite and Earth system model estimates of global terrestrial CO_2 fertilization, Nature Climate Change, 6, 306, 2016.

Stevens, N., Lehmann, C. E., Murphy, B. P., and Durigan, G.: Savanna woody encroachment is widespread across three continents, Glob Chang Biol, 23, 235-244, 2017.

Still, C. J., Berry, J. A., Collatz, G. J., and DeFries, R. S.: Global distribution of C3 and C4 vegetation: Carbon cycle implications, Global Biogeochemical Cycles, 17, 6-1-6-14, 2003.

Tape, K., Sturm, M., and Racine, C.: The evidence for shrub expansion in Northern Alaska and the Pan-Arctic, Global Change Biology, 12, 686-702, 2006.

Thomas, N., and Nigam, S.: Twentieth-Century Climate Change over Africa: Seasonal Hydroclimate Trends and Sahara Desert Expansion, Journal of Climate, 31, 3349-3370, 2018.

Williams, I. N., Torn, M. S., Riley, W. J., and Wehner, M. F.: Impacts of climate extremes on gross primary production under global warming. Environmental Research Letters, 9(9), 094011. 2014.

Woodward, F. I., and Lomas, M. R.: Vegetation dynamics--simulating responses to climatic change, Biol Rev Camb Philos Soc, 79, 643-670, 2004.

Wu, Z. D., Ahlstrom, A., Smith, B., Ardo, J., Eklundh, L., Fensholt, R., and Lehsten, V.: Climate data induced uncertainty in model-based estimations of terrestrial primary productivity, Environmental Research Letters, 12, 064013, 2017.

Xiao, Z., Liang, S., Wang, J., Chen, P., Yin, X., Zhang, L. Q., and Song, J.: Use of General Regression Neural Networks for Generating the GLASS Leaf Area Index Product From Time-Series MODIS Surface Reflectance, Ieee Transactions on Geoscience and Remote Sensing, 52, 209-223, 2014.

Xu, L., Myneni, R. B., Chapin Iii, F. S., Callaghan, T. V., Pinzon, J. E., Tucker, C. J., and Euskirchen, E. S: Temperature and vegetation seasonality diminishment over northern lands. Nature Climate Change, 3(6), 581. 2013

Xue, Y., Sellers, P. J., Kinter, J. L., and Shukla, J.: A Simplified Biosphere Model for Global Climate Studies, Journal of Climate, 4(3), 345-364, 1991.

Xue, Y., Juang, H. M. H., Li, W. P., Prince, S., DeFries, R., Jiao, Y., and Vasic, R.: Role of land surface processes in monsoon development: East Asia and West Africa, J Geophys Res-Atmos, 109(D3), 2004a.

Xue, Y., De Sales, F., Vasic, R., Mechoso, C. R., Arakawa, A., and Prince, S.: Global and Seasonal Assessment of Interactions between Climate and Vegetation Biophysical Processes: A GCM Study with Different Land-Vegetation Representations, Journal of Climate, 23, 1411-1433, 2010.

Xue, Y., Zeng, F., and Schlosser, C. A.: SSiB and its sensitivity to soil properties - A case study using HAPEX-Mobilhy data, Global and Planetary Change, 13, 183-194, 1996.

Yue, X., Unger, N., and Zheng, Y.: Distinguishing the drivers of trends in land carbon fluxes and plant volatile emissions over the past 3 decades, Atmospheric Chemistry and Physics, 15, 11931-11948, 2015.

Xue, Y., F. De Sales, W.K-M Lau, A. Boone, K.-M. Kim, C.R. Mechoso, G. Wang, F. Kucharski, K. Schiro, M. Hosaka, S. Li, L.M. Druyan, I. Seidou Sanda, W. Thiaw, N. Zeng, R.E. Comer, Y.-K. Lim, S. Mahanama, G. Song, Y. Gu, S.M. Hagos, M. Chin, S. Schubert, P. Dirmeyer, L.R. Leung, E. Kalnay, A. Kitoh, C.-H. Lu, N.M. Mahowald, and Z. Zhang: West African monsoon decadal variability and drought and surface-related forcings: Second West African Monsoon Modeling and Evaluation Project Experiment (WAMME II). Clim. Dyn., 47, no. 11, 3517-3545, 2016.

Zaehle, S., and Friend, A. D.: Carbon and nitrogen cycle dynamics in the O-CN land surface model: 1. Model description, site-scale evaluation, and sensitivity to parameter estimates, Global Biogeochemical Cycles, 24, 2010.

Zeng, F., Collatz, G. J., Pinzon, J. E., and Ivanoff, A.: Evaluating and Quantifying the Climate-Driven Interannual Variability in Global Inventory Modeling and Mapping Studies (GIMMS) Normalized Difference Vegetation Index (NDVI3g) at Global Scales, Remote Sensing, 5, 3918-3950, 2013.

Zeng, N., Mariotti, A., and Wetzel, P.: Terrestrial mechanisms of interannual CO_2 variability, Global Biogeochemical Cycles, 19, 2005.

Zeng, X., Zeng, X., and Barlage, M.: Growing temperate shrubs over arid and semiarid regions in the Community Land Model-Dynamic Global Vegetation Model, Global Biogeochemical Cycles, 22, 2008.

Zhan, X., Xue, Y., and Collatz, G. J.: An analytical approach for estimating CO_2 and heat fluxes over the Amazonian region, Ecological Modelling, 162, 97-117, 2003.

Zhang, Z., Xue, Y., MacDonald, G., Cox, P., and Collatz, G.: Investigation of North American vegetation variability under recent climate: A study using the SSiB4/TRIFFID biophysical/dynamic vegetation model, Journal of Geophysical Research-Atmospheres, 120, 1300-1321, 2015.

Zhu, Z., Piao, S., Lian, X., Myneni, R. B., Peng, S., and Yang, H.: Attribution of seasonal leaf area index trends in the northern latitudes with "optimally" integrated ecosystem models, Glob Chang Biol, 23, 4798-4813, 2017.

Zhu, Z., Bi, J., Pan, Y., Ganguly, S., Anav, A., Xu, L., Samanta, A., Piao, S., Nemani, R. R, and Myneni, R. B.: Global Data Sets of Vegetation Leaf Area Index (LAI)3g and Fraction of Photosynthetically Active Radiation (FPAR)3g Derived from Global Inventory Modeling and Mapping Studies (GIMMS) Normalized Difference Vegetation Index (NDVI3g) for the Period 1981 to 2011, Remote Sensing, 5, 927-948, 2013.

Zhu, Z., Piao, S., Myneni, R. B., Huang, M., Zeng, Z., Canadell, J. G., Ciais, P., Sitch, S., Friedlingstein, P., Arneth, A., Cao, C., Cheng, L., Kato, E., Koven, C., Li, Y., Lian, X., Liu, Y. W., Liu, R. G., Mao, J. F., Pan, Y. Z., Peng, S. S., Penuelas, J., Poulter, B., Pugh, T. A. M., Stocker, B. D., Viovy, N., Wang, X., Wang, Y., Xiao, Z., Yang, H., Zaehle, S., and Zeng, N.: Greening of the Earth and its drivers, Nature Climate Change, 6, 791-+, 2016.

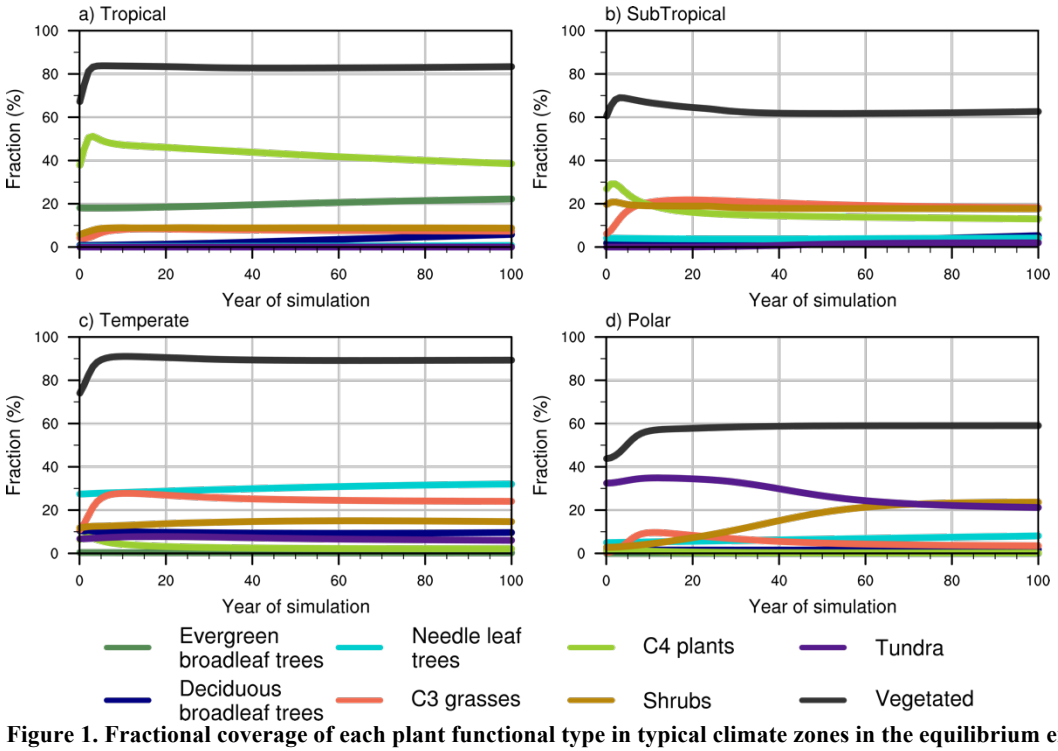

Figure 1. Fractional coverage of each plant functional type in typical climate zones in the equilibrium experiment

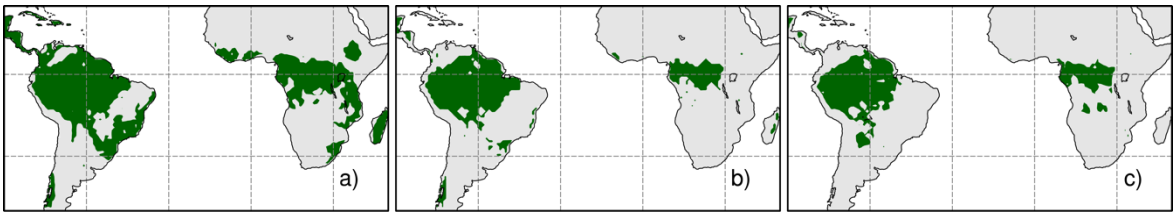

Figure 2. Tree dominated areas of a) unchanged large-scale disturbance experiment, b) parameter updated experiment and c) GLC2000

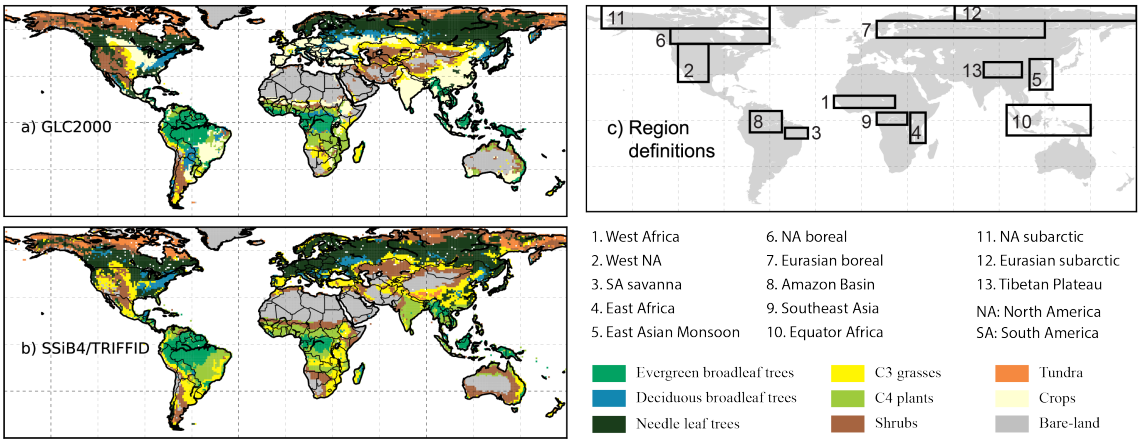

Figure 3. Dominant vegetation type comparison between a) GLC2000 and b) SSiB4/TRIFFID, and c) Region definitions.

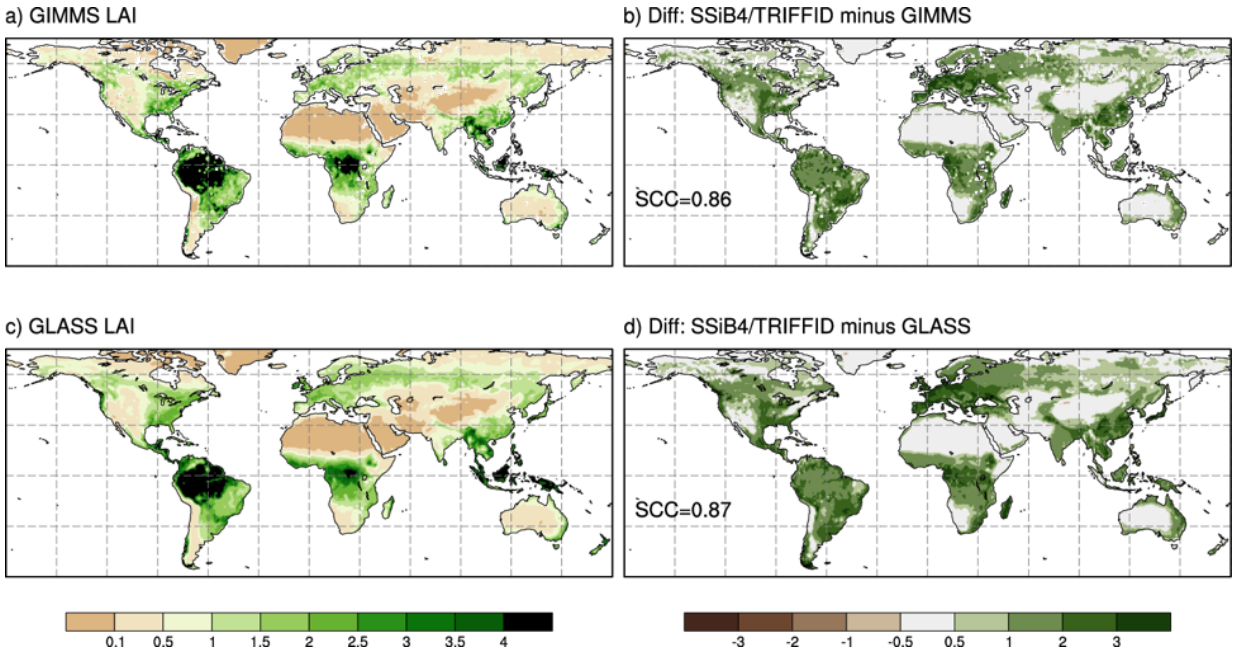

Figure 4. 1982-2007 average leaf area index comparison for a) GIMMS LAI, c) GLASS LAI, and difference between SSiB4/TRIFFID and b) GIMMS and d) GLASS. SCC indicates the spatial correlation coefficient between model simulation and satellite-derived datasets.

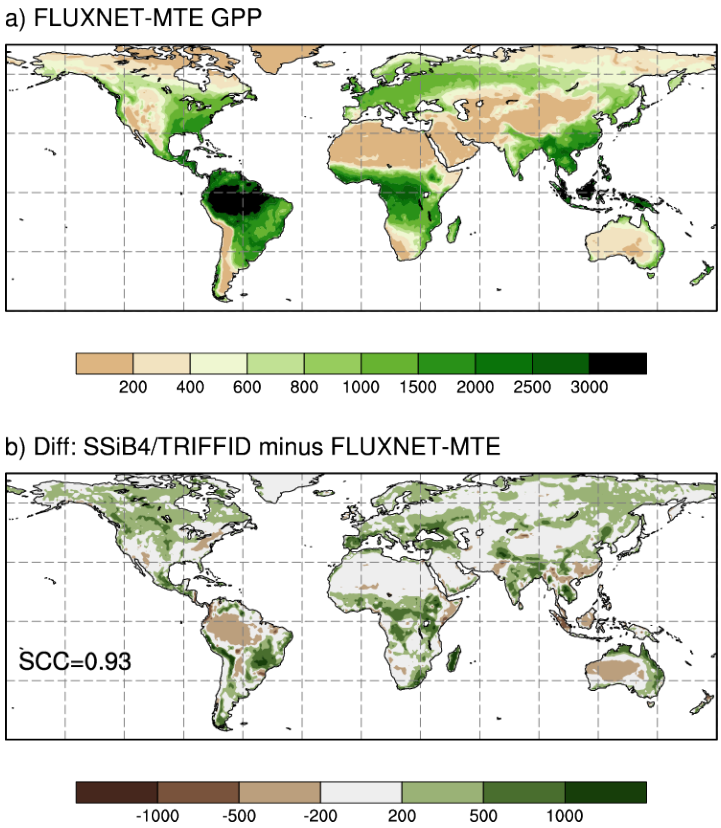

Figure 5. 1982-2007 average gross primary product comparison for a) FLUXNET-MTE GPP, and b) different between SSiB4/TRIFFID and FLUXNET-MTE GPP. SCC indicates the spatial correlation coefficient.

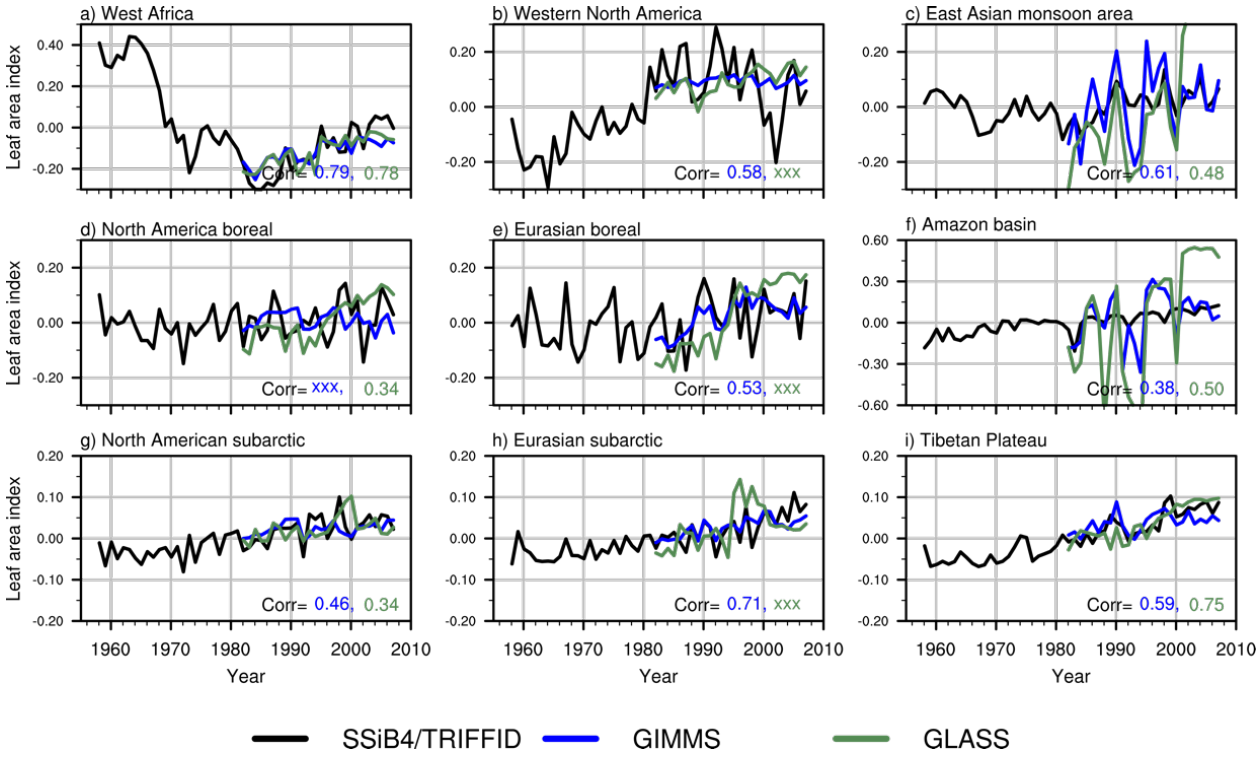

Figure 6. Comparison of standardized LAI anomalies between simulation and observations for 9 sub-regions. Corr indicates the interannual correlation coefficient simulated (in black) LAI against the GIMMS (in blue) and the GLASS (in green). Only significant values (P<0.1) are shown, whereas non-significant values are masked by xxx

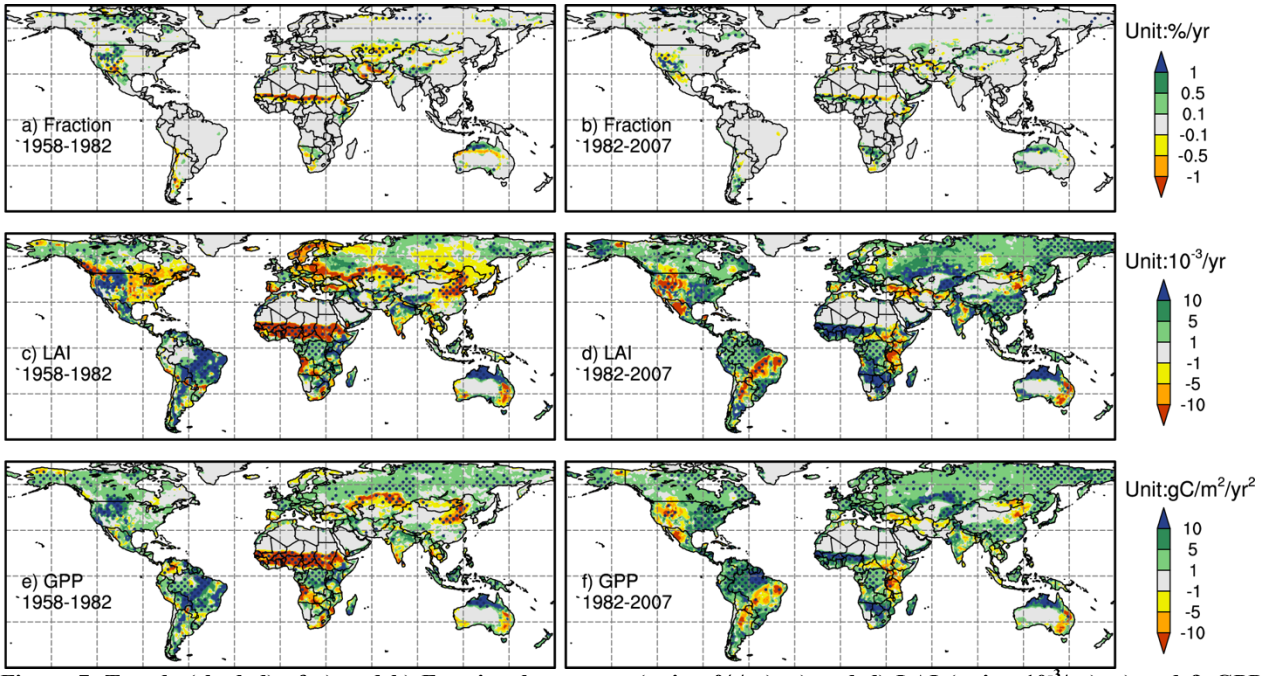

Figure 7. Trends (shaded) of a) and b) Fractional coverage (units: %/yr), c) and d) LAI (units: 10^{-3}/yr), e) and f) GPP (units: $gC/m^2/yr^2$). The left three panels are for 1958-1982 and the right three panels are for 1982-2007. The dots indicate the areas with significance level at P< 0.05 (Mann-Kendall test).

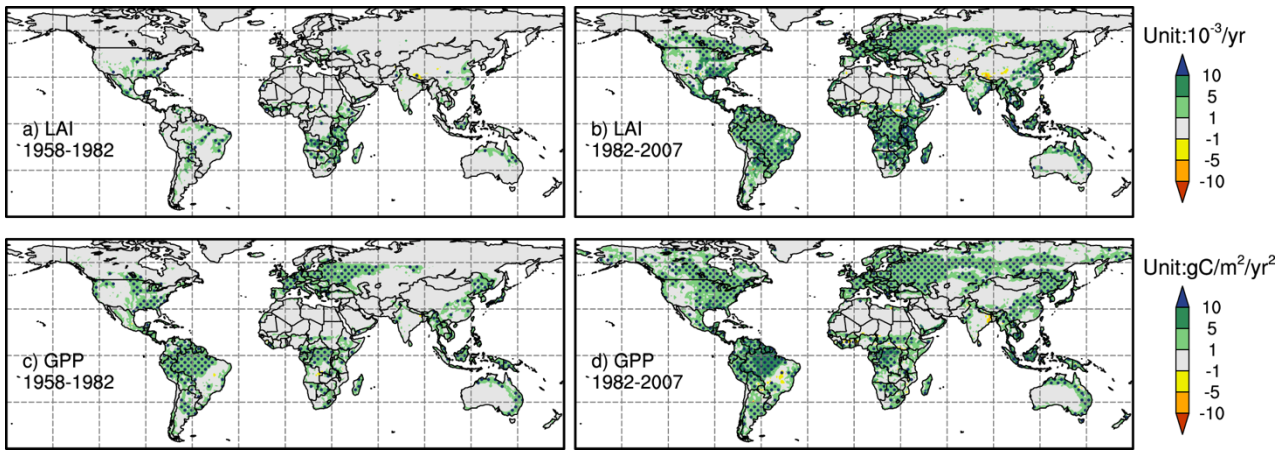

Figure 8. CO_2 effect on the trends (shaded) of a) and b) LAI (units: 10^{-3}/yr), and c) and d) GPP (units: $gC/m^2/yr^2$). The left two panels are for 1958-1982 and the right two panels are for 1982-2007.

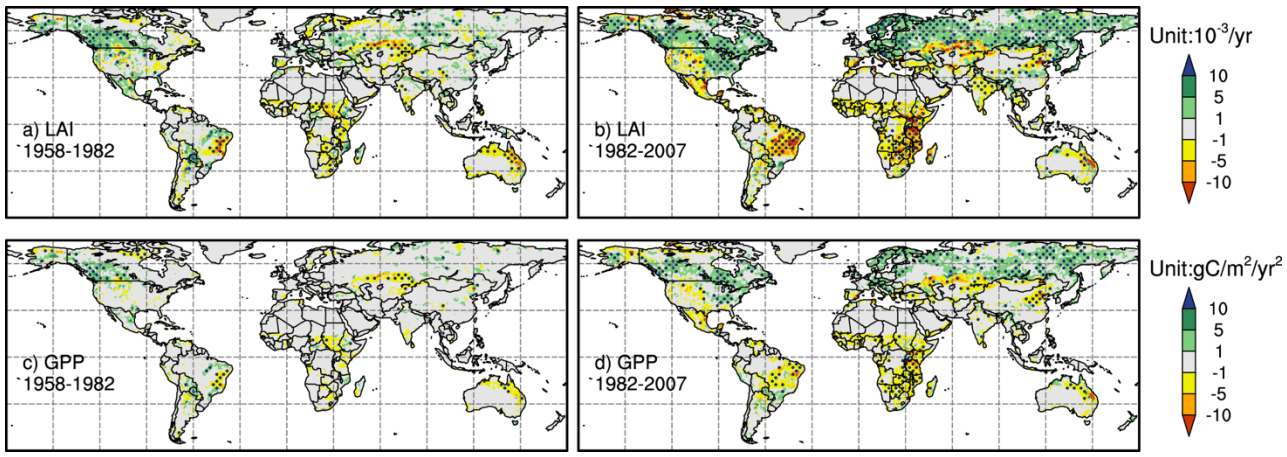

Figure 9. Same as Figure 8, but for warming effect.

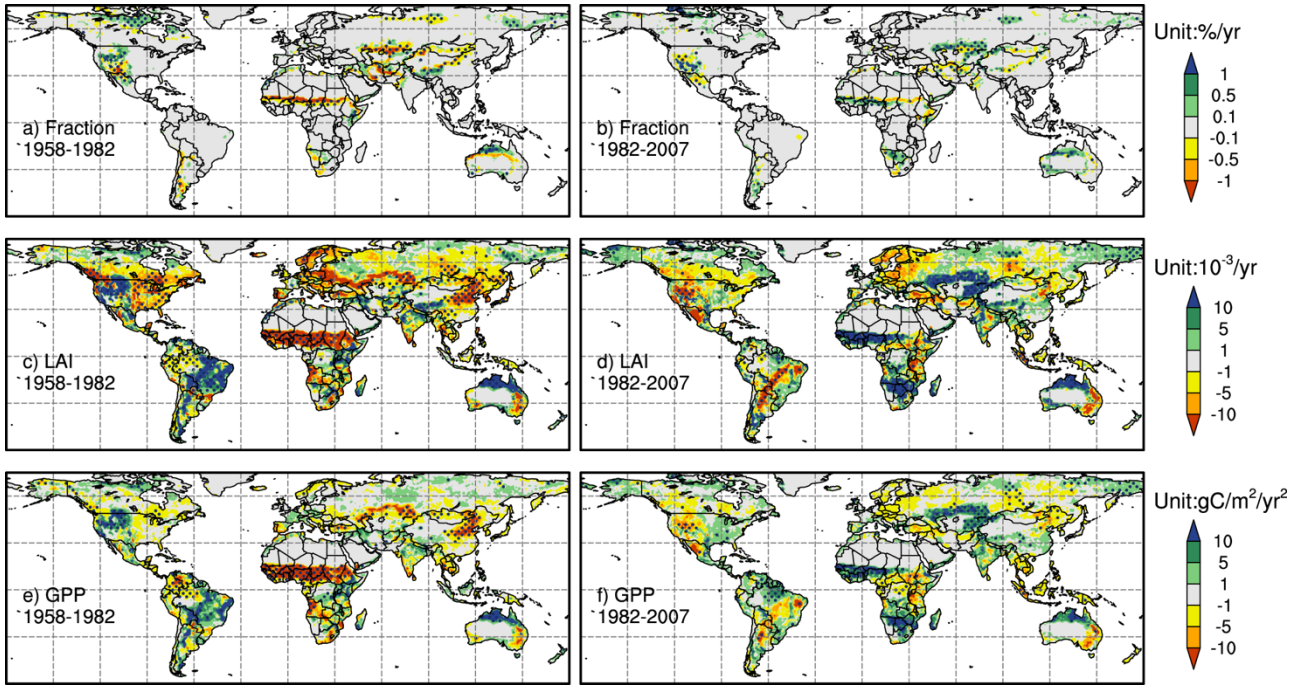

Figure 10. Same as Figure 8, but for climate viability effect and also including the effects on fractional coverage (units: %/yr)

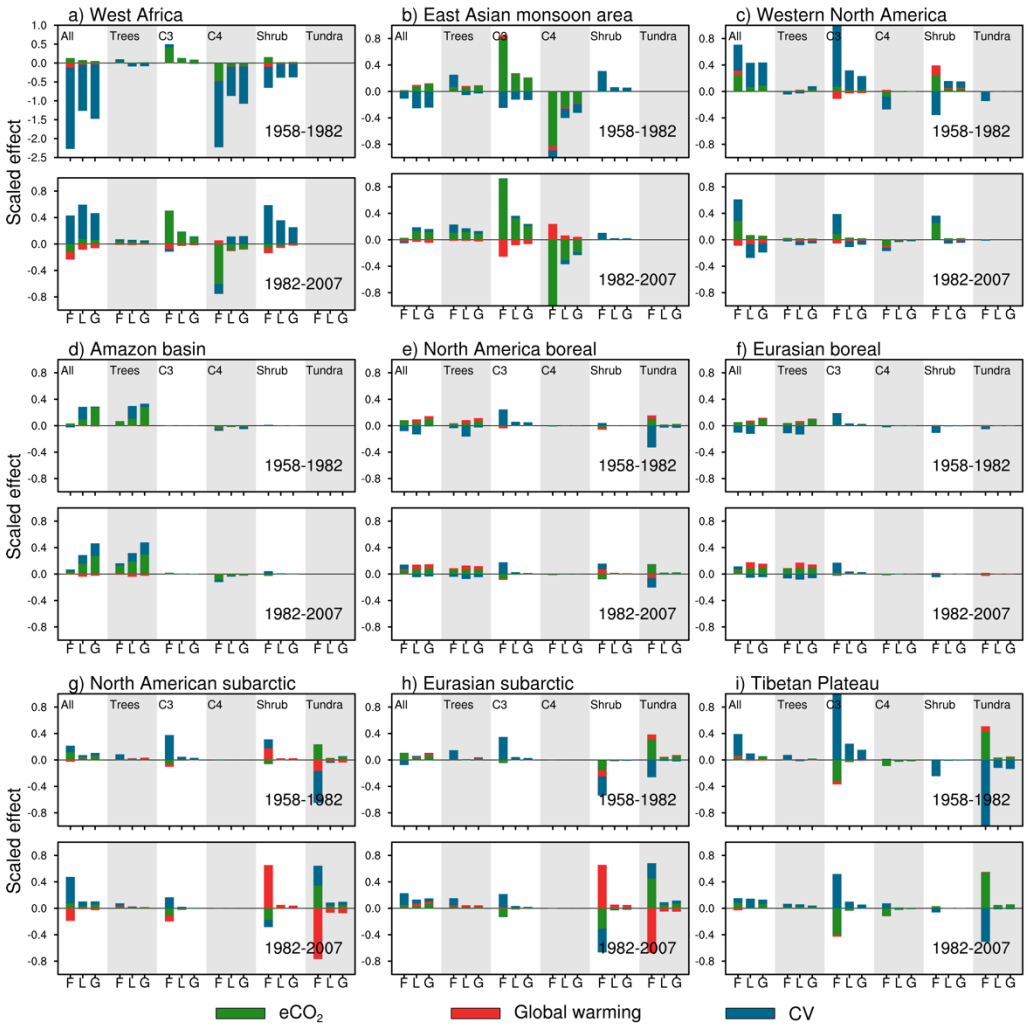

Figure 11. Contribution of each factor on FRAC (denoted as "F"), LAI (denoted as "L"), and GPP (denoted as "G") trend over sub-regions. The upper panel in each figure is for trends during 1951-1982 and the lower panel is for trends during 1982-2007. The effects of eCO_2, global warming and CV are shown in green, red, and blue bars, separately. Each column shows the effects on all PFTs (All), trees, C3 grass (C3), C4 plant (C4), shrub, and tundra, separately. The numbers for FRAC, LAI, and GPP are normalized by dividing the standard deviation of global average in the control experiment.

Table 1. Experimental design

Equilibrium simulation	Description	Real-forcing simulation	Description
Control experiment	Fixed CO_2 concentration at 1948 level and driven by climatological forcing for 100 years	**Control experiment**	Transient CO_2 concentration and meteorological forcing for the period of 1948-2007
Parameter updated experiment	Adjusting large scale disturbance for trees	**Fixed-CO_2**	The same as Control experiment except for fixed CO_2 concentration at 1948 level
		Detrend-Temp	The same as Control experiment except for no global warming trend

Table 2. Location for study areas

Regions	Sub-regions	Location
Arid and Semi-Arid Areas	West Africa	8°N~16°N, 18°W~22°E
	Western North America	25°N~50°N, 120°W~100°W
	South American savanna	12°S~5°S, 50°W~35°W
	East Africa	15°S~5°N, 32°E~42°E
Monsoon Area	East Asian monsoon area	20°N~40°N, 110°E~125°E
Northern Hemisphere boreal areas	North America boreal	50°N~60°N, 125°W~60°W
	Eurasian boreal	54°N~65°N, 10°E~120°E
Equator areas	Amazon basin	8°S~6°N, 73°W~52°W
	Southeast Asia	10°S~10°N, 95°E~150°E
	Equator Africa	3°S~5°N, 10°E~30°E
Subarctic areas	North American subarctic	60°N~75°N, 170°W~60°W
	Eurasian subarctic	65°N~75N, 60°E~180°E
Tibetan Plateau	Tibetan Plateau	28°N~38°N, 80°E~105°E

Table 3. Statistics for the comparison between SSiB4/TRIFFID simulated and observation-based LAI and GPP

Regions	Sub-regions	LAI Mean (m^2/m^2)			LAI TCC		GPP Mean ($gC/m^2/yr$)		GPP TCC
		GIMMS	GLASS	SSiB4/TRIFFID	GLASS	GLASS	MTE	SSiB4/TRIFFID	MTE
Arid and Semi-Arid Areas	West Africa	0.92	0.86	1.75	0.80**	0.79**	759.97	970.82	0.80**
	Western North America	0.57	0.46	1.27	0.58**		404.65	520.91	0.70**
	South American savanna	1.85	1.82	3.27	0.57**	0.54**	1615.28	1823.22	0.65**
	East Africa	1.49	1.38	2.95	0.46**		1188.67	1487.25	0.63**
Monsoon Area	East Asian monsoon area	1.59	1.31	3.58	0.61**	0.48**	1402.44	1503.18	0.51**
Northern Hemisphere boreal areas	North America boreal	0.80	0.91	1.94		0.34*	544.45	867.94	0.83**
	Eurasian boreal	1.15	1.26	2.46	0.52**		857.16	1036.47	0.70**
Equator areas	Amazon basin	4.18	4.28	6.15	0.38*	0.50**	2992.29	2820.73	
	Southeast Asia	4.00	3.16	4.82		0.38*	2792.95	2628.02	
	Equator Africa	3.86	3.48	6.09	0.36*	0.70**	2535.6	2833.9	
Subarctic areas	North American subarctic	0.37	0.38	0.78	0.46**	0.35*	256.46	438.18	0.72**
	Eurasian subarctic	0.35	0.44	0.92	0.71**		345.82	539.41	0.64**
Tibetan Plateau	Tibetan Plateau	0.52	0.43	1.29	0.58**	0.74**	323.12	546.2	0.49**

Note: * indicates the $p<0.1$ and ** indicates the $p<0.05$

Table 4. Linear trend of vegetation FRAC, LAI and GPP changes during P1 (1958-1982) and P2 (1982-2007) in sub-regions (1)

Regions	Var.	Total		Trees		C3 grass		C4 plant		Shrub		Tundra	
		P1	P2	P1	P2	P1	P2	P1	P2	P1	P2	P1	P2
West Africa	**FRAC**	-4.14				**0.96**	**0.99**	-4.33	-1.71	-0.96	**1.1**		
	LAI	-2.58	**1.37**			**0.28**	**0.43**	-1.9		-0.79	**0.8**		
	GPP	-18.54	8.02	-0.84	**0.86**	**0.92**	**1.9**	-14.09		-4.53	**4.49**		
East Asian Monsoon area	**FRAC**			**0.51**	**0.56**	**1.19**	**1.72**	-2.49	-2.6	**0.63**			
	LAI	-0.34	**0.43**		**0.44**	**0.34**	**0.76**	-0.9	-0.83				
	GPP	-1.61	**2.39**	**0.84**	**2.17**	**1.06**	**3.51**	-4.35	-3.73	**0.84**	**0.44**		
Western North America	**FRAC**	**1.34**	**1.38**			**2.18**	**0.83**	-0.48	-0.38		**0.96**		
	LAI	**0.96**	-0.58			**0.65**	-0.23			**0.34**			
	GPP	**5.66**	-2.73	**1.02**	-0.74	**2.76**	-1.12		-0.42	**1.95**			
Amazon basin	**FRAC**				**0.37**								
	LAI	**0.57**	**0.66**	**0.61**	**0.74**								
	GPP	**3.49**	**8.7**	**4.08**	**8.93**			-0.67	-0.39				
North American boreal	**FRAC**		**0.36**			**0.4**						-0.34	
	LAI		**0.25**										
	GPP	**1.77**	**2.2**	**1.17**	**1.41**	**0.64**							**0.33**
Eurasian boreal	**FRAC**		**0.29**			**0.37**	**0.37**						
	LAI		**0.33**		**0.23**								
	GPP	**1.58**	**2.17**	**1.42**	**1.61**	**0.35**	**0.58**						
North American subarctic	**FRAC**	**0.35**	**0.69**	**0.16**	**0.18**	**0.51**				**0.46**	**0.88**	-0.76	-0.29
	LAI		**0.23**										
	GPP	**1.33**	**1.47**	**0.43**	**0.35**	**0.34**				**0.32**	**0.59**		**0.5**
Eurasian subarctic	**FRAC**		**0.59**	**0.29**	**0.39**	**0.58**	**0.20**			-1.02			
	LAI		**0.35**										
	GPP	**1.42**	**2.97**	**0.52**	**0.85**	**0.36**					**0.56**	**0.69**	**1.31**
Tibetan Plateau	**FRAC**	**0.83**	**0.32**			**4.51**				-0.44		-3.26	
	LAI	**0.2**	**0.39**			**0.48**							
	GPP	**0.68**	**2.61**		**0.78**	**1.9**	**0.98**					-1.14	**0.93**

(1) Only significant values (P<0.1 in Mann-Kendall test) are shown, positive trends are in bold. Numbers are scaled by multiplying 10 for FRAC and 1000 for LAI.

Table 5. Climate drivers and eCO_2 effect on the trends of FRAC, LAI and GPP during P1 (1958-1982) and P2 (1982-2007) in sub-regions regarding to their regional average [(1)(2)]

Regions	Var.	Total		Elevated CO_2 concentration		Global warming		Climate variability	
		P1	P2	P1	P2	P1	P2	P1	P2
West Africa	**FRAC**	-0.51						-0.51	**0.14**
	LAI	-1.47	**0.78**	**0.10**	**0.12**	-0.05	-0.13	-1.52	**0.80**
	GPP	-1.91	**0.83**	**0.07**	**0.12**	-0.05	-0.13	-1.94	**0.83**
East Asian Monsoon area	**FRAC**								
	LAI	-0.10	**0.12**	**0.05**	**0.10**			-0.16	
	GPP	-0.11	**0.16**	**0.10**	**0.16**		-0.06	-0.21	**0.06**
Western North America	**FRAC**	**0.18**	**0.18**	**0.07**	**0.10**			**0.09**	**0.12**
	LAI	**0.75**	-0.45	**0.11**	**0.14**		-0.14	**0.64**	-0.46
	GPP	**1.09**	-0.52	**0.22**	**0.23**		-0.19	**0.88**	-0.56
Amazon basin	**FRAC**								
	LAI	**0.09**	**0.11**	**0.03**	**0.07**			**0.06**	**0.06**
	GPP	**0.12**	**0.31**	**0.13**	**0.19**				**0.14**
North American boreal	**FRAC**		**0.04**						
	LAI		**0.13**	**0.05**	**0.10**	**0.06**	**0.10**	-0.14	-0.07
	GPP	**0.20**	**0.25**	**0.14**	**0.20**	**0.08**	**0.14**		-0.08
Eurasian boreal	**FRAC**		**0.03**						
	LAI		**0.13**		**0.10**		**0.10**	-0.11	-0.06
	GPP	**0.15**	**0.21**	**0.13**	**0.18**		**0.11**		-0.09
North American subarctic	**FRAC**	**0.05**	**0.09**				-0.06		**0.13**
	LAI		**0.30**	**0.07**	**0.10**			**0.09**	**0.25**
	GPP	**0.30**	**0.34**	**0.17**	**0.24**		-0.12	**0.12**	**0.22**
Eurasian subarctic	**FRAC**		**0.06**						**0.05**
	LAI		**0.39**	**0.07**	**0.10**		**0.11**		**0.18**
	GPP	**0.26**	**0.55**	**0.17**	**0.25**	**0.06**	**0.13**		**0.18**
Tibetan Plateau	**FRAC**	**0.12**	**0.04**					**0.10**	
	LAI	**0.16**	**0.31**					**0.17**	**0.28**
	GPP	**0.13**	**0.48**	**0.12**	**0.21**				**0.26**

(1) percentage trend for FRAC: $Trend_{FRAC}/(grid\ total\ vegetated\ FRAC) * 100\%$
percentage trend for LAI and GPP: $Trend_{var}/(grid\ averaged) * 100\%$, where *var* stands for LAI or GPP. Units for all three variables are %/yr

(2) Only significant values (P<0.05 in Mann-Kendall test) are shown, positive trends are in bold